

Ergotropic Mpemba crossings in finite-dimensional quantum batteries

Triyas Sapui¹, Tanoy Kanti Konar^{1,2}, Aditi Sen (De)¹

¹*Harish-Chandra Research Institute, A CI of Homi Bhabha National Institute, Chhatnag Road, Jhunsi, Prayagraj - 211019, India*

²*Institute of Theoretical Physics, Faculty of Physics, Astronomy, and Computer Science, Jagiellonian University in Krakow, Stanisława Łojasiewicza street 11, PL-30-348 Kraków, Poland*

The quantum Mpemba effect is a counterintuitive phenomenon in which a state initially farther from equilibrium relaxes more rapidly than one that starts nearer to equilibrium. In the context of finite-dimensional quantum batteries interacting with an environment, we introduce the notion of an ergotropic Mpemba crossing (EMC), defined by the intersection of ergotropy trajectories during the dynamics. For qubit batteries subjected to amplitude damping noise, we derive a condition for the occurrence of EMC in terms of the relative coherence of the initial states and fully characterize the region of state space that exhibits EMC with respect to a fixed reference state. Interestingly, our analysis reveals that under anisotropic Pauli noise, the emergence of EMC is jointly governed by the coherence and the energy of the initial states. To elucidate the physical origin of EMC, we decompose ergotropy into coherent and incoherent contributions and show that, in qubit systems, coherent component plays a crucial role for EMC, an observation that strikingly does not extend to three-level batteries. Further, by extending our analysis to non-Markovian environments, we demonstrate that, unlike the Markovian case, non-Markovian dynamics can give rise to multiple Mpemba crossings, with the total number of crossings always being odd. Moreover, analyzing the connection between the EMC and the conventional state Mpemba effect reveals that, for qubits, an EMC necessarily entails a state Mpemba crossing while this correspondence breaks down for qutrits, where EMCs may arise without any state Mpemba crossing.

I. INTRODUCTION

The Mpemba effect is a counterintuitive thermodynamic phenomenon in which a system prepared at a higher initial temperature relaxes to equilibrium faster than an initially colder one. It was first observed experimentally by Mpemba and Osborne [1] and a systematic theoretical framework for classical systems coupled to thermal environments was subsequently developed [2]. In the quantum domain, the Mpemba-like behavior has been explored primarily in nonequilibrium settings, such as random quantum circuits [3, 4] and interacting many-body systems [5–8]. For open quantum systems, the phenomenon, often termed as *thermal Mpemba effect* has been identified in both Markovian [9–17] and non-Markovian dynamics [18, 19]. In the Markovian case, exponential acceleration of relaxation has been demonstrated via global rotations in a variety of models, including the Dicke model [9], spin chains [20–23], quantum dots [24–26], fermionic systems [25], and bosonic setups [27, 28], with relaxation typically quantified using distance measures such as the Hilbert–Schmidt and trace distances. The role of memory effects in the non-Markovian regime has also been extensively analyzed [29–31] along with studies on the typicality of relaxation under environmental coupling [32] (cf. [33–36]). Crucially, these theoretical insights have been supported by experimental realizations in platforms such as trapped-ion simulators [37] and nuclear magnetic resonance platforms [38, 39].

In the quest to understand thermodynamic principles at the microscopic scale, quantum batteries, quantum-mechanical energy storage devices [40], have emerged as a key platform for identifying genuine quantum advantages in energy storage and delivery. Over the past few years, extensive research has explored various aspects of quantum batteries, including collective and high-power charging protocols [41–43], the role of quantum correlations [44–46], fundamental bounds on capacity and power [47, 48], and connections to quantum speed

limits [49–51]. In realistic settings, however, quantum batteries inevitably interact with their environment, leading to dissipation and decoherence. This has motivated a growing body of work examining how environmental effects influence the charging and discharging dynamics of quantum batteries [52–66].

Within this context, a natural and intriguing question arises: “can quantum battery performance metrics, such as ergotropy, exhibit Mpemba-like behavior?” Recent studies have answered this affirmatively by demonstrating that a continuous-variable (CV) quantum battery subject to environmental noise can exhibit a Mpemba effect [67], where a more highly charged squeezed state discharges faster than a less charged displaced state. This phenomenon has been further extended to non-Markovian CV dynamics, where multiple crossings in ergotropy, termed the *quasi-ergotropic Mpemba effect*, have also been observed [30]. Related Mpemba-like behavior has also been reported in other quantum thermodynamic settings, including self-contained quantum refrigerators [68], quantum thermometry where Mpemba crossings define an operational advantage over equilibrium-based protocols [69], underscoring the broad relevance of Mpemba physics in quantum technologies (see also Refs. [70, 71]).

In this work, we exhibit that ergotropic Mpemba crossings (EMC) are not exclusive to continuous-variable systems but can also emerge in discrete-variable quantum batteries. Focusing on a single-qubit battery subject to Markovian noise, modeled by generalized amplitude damping and Pauli channels, we derive conditions expressed in terms of properties of the initial states for the occurrence of EMC. For amplitude damping noise, we rigorously prove that two arbitrary initial states with ordered ergotropies cannot manifest EMC if their l_1 -norm of coherence follows the same ordering. In contrast, for Pauli noise, the appearance of EMC is jointly governed by the relative coherence and energy of the initial states. To uncover the physical origin of this effect, we decompose

ergotropy into coherent and incoherent contributions. For qubits, we find that the incoherent component decays exponentially, while the coherent one delays relaxation toward the steady state, thereby enabling EMC. Extending our analysis to higher-dimensional batteries, particularly qutrits, we demonstrate that EMC can arise even in the absence of coherent ergotropy, underscoring the essential role of additional energy levels. In particular, we determine the conditions on the initial probability distribution of energy levels that gives rise to EMC. Furthermore, under non-Markovian amplitude damping noise, we identify the state-dependent conditions leading to EMC and prove that only an odd number of ergotropic crossings can occur. We examine the relationship between the ergotropic Mpemba effect and the conventional state Mpemba effect. We show that for qubit systems, the ergotropy Mpemba effect implies the state Mpemba effect, however, the converse does not generally hold for three-level systems.

This paper is structured as follows. Sec. II provides an overview of the ergotropic Mpemba effect and demonstrates the criteria to find ergotropy Mpemba crossing for a two-qubit state with consideration of both amplitude damping and the anisotropic Pauli channel. In Sec. III, we illustrate that the occurrence of EMC due to the trade-off relationship between the incoherent and coherent parts of the ergotropy itself. Sec. IV, depicts the EMC in a qutrit system, specifically in a diagonal qutrit system. In Sec. V, we demonstrate the emergence of EMC in a non-Markovian setup with multiple crossings. Before concluding remarks in Sec. VII, we connect the ergotropic Mpemba crossing with the state Mpemba effect in Sec. VI.

II. CRITERIA FOR DETECTING SINGLE-QUBIT ERGOTROPIC MPEMBA EFFECT

The Mpemba effect naturally underscores the influence of the environment on physical systems. Such an effect can, in principle, be observed for any quantity associated with a quantum state, such as entanglement or coherence. While early studies focused on how the state itself approaches equilibrium, these derived quantities or resources need not follow the same relaxation behavior as the state (cf. [11, 72]). We here concentrate on the ergotropic Mpemba effect in a finite-dimensional quantum battery.

1. Concept of ergotropic Mpemba crossing

Before presenting the results, we introduce the concept of the ergotropic Mpemba crossing, which serves as the central identifier for the Mpemba effect in an energy storage device.

Ergotropy. The maximum extractable work from the battery through unitary operation, called *ergotropy* [40] is defined as

$$\mathcal{E}(\rho) = \text{Tr}[\rho H_B] - \min_U \text{Tr}[U \rho U^\dagger H_B], \quad (1)$$

where ρ is an arbitrary state of the battery Hamiltonian, $H_B = \sum_{i=1}^n \epsilon_i |\epsilon_i\rangle\langle\epsilon_i|$ [73] where $\epsilon_i \geq \epsilon_{i-1}$ for all i . The

second term in Eq. (1) represents the energy corresponding to the passive state, ρ_π , of ρ . If $\rho = \sum_{i=1}^n p_i |\epsilon_i\rangle\langle\epsilon_i|$ where $p_i \geq p_{i+1}$ for all i , the passive state is given by $\rho_\pi = \sum_{i=1}^n p_i |\epsilon_i\rangle\langle\epsilon_i|$ where $\{|\epsilon_i\rangle\}$ is the set of energy eigenstates of the battery Hamiltonian. Using this, Eq. (1) reduces to $\mathcal{E}(\rho) = \text{Tr}[\rho H_B] - \sum p_i \epsilon_i$.

Ergotropic Mpemba crossing. The Mpemba-type behavior discussed here arises in the discharging dynamics of a quantum battery made up with a single d -dimensional system. When two initial states with different ergotropies are coupled to a Markovian bath, it may happen that the state with a higher ergotropy discharges faster than the one with a lower ergotropy. This phenomenon can be called the *ergotropic Mpemba effect* and the corresponding intersection point of the two ergotropy curves at finite time is referred to as the *ergotropic Mpemba crossing* (EMC). In a continuous-variable quantum battery, it was shown that a highly charged state may discharge more rapidly, with the discharge rate being determined by the squeezing and displacement properties of the initial state [67].

In our work, we consider that the battery is under the influence of two different Markovian noises – (1) generalized amplitude damping channel (gADC) and (2) anisotropic Pauli channel. In the former case, the battery is influenced by a thermal bath with temperature, T and the governing Gorini–Kossakowski–Sudarshan–Lindblad (GKSL) master equation [75–77] reads

$$\frac{d\rho}{dt} = -i[H_B, \rho] + \gamma_- \mathcal{D}[\sigma_-] + \gamma_+ \mathcal{D}[\sigma_+], \quad (2)$$

where $\mathcal{D}[A] = A\rho A^\dagger - \frac{1}{2}\{A^\dagger A, \rho\}$, $\gamma_\pm \geq 0$ is the decay strength of the ADC, and $\sigma_\pm = (\sigma_x \pm i\sigma_y)/2$ is the Lindblad operator. Here $\gamma_+ = \gamma_- e^{-\beta H_B}$ and the steady state of the Lindblad channel is a thermal state, $\rho_{ss} = \frac{e^{-\beta H_B}}{\text{Tr}[e^{-\beta H_B}]}$, where $\beta = 1/k_B T$ is the inverse temperature of the bath with k_B being the Boltzmann constant. If the bath temperature is taken to be vanishing, i.e., $T = 0$, implying $\gamma_+ = 0$, the corresponding steady state is the ground state of the Hamiltonian, H_B .

Unlike gADC, let us consider another channel, namely *Pauli* channel. The evolution of the qubit is given as

$$\frac{d\rho}{dt} = -i[H_B, \rho] + \gamma_x \mathcal{D}[\sigma_x] + \gamma_y \mathcal{D}[\sigma_y] + \gamma_z \mathcal{D}[\sigma_z], \quad (3)$$

where the dissipation strength $\gamma_{x,y,z} \geq 0$. We consider $\gamma_x = \gamma_y = \gamma_\perp$ with arbitrary value of γ_z . For this case, the dynamics is again phase covariant and is referred to as anisotropic Pauli noise. So, we can divide three regimes where $\gamma_\perp > \gamma_z$, $\gamma_\perp = \gamma_z$ and $\gamma_\perp < \gamma_z$ which depicts the strength of the noise in each direction. Interestingly, for all the cases, the steady state is given by $\mathbb{I}_2/2$.

In order to study EMC, let us consider ergotropies of two initial states, ρ_1 , and ρ_2 , as $\mathcal{E}_1 \equiv \mathcal{E}(\rho_1)$ and $\mathcal{E}_2 \equiv \mathcal{E}(\rho_2)$ respectively, with $\mathcal{E}_1 > \mathcal{E}_2$. When the system is coupled to a dissipative bath, the ergotropy typically decreases with time and eventually saturates to a steady state value. We call the

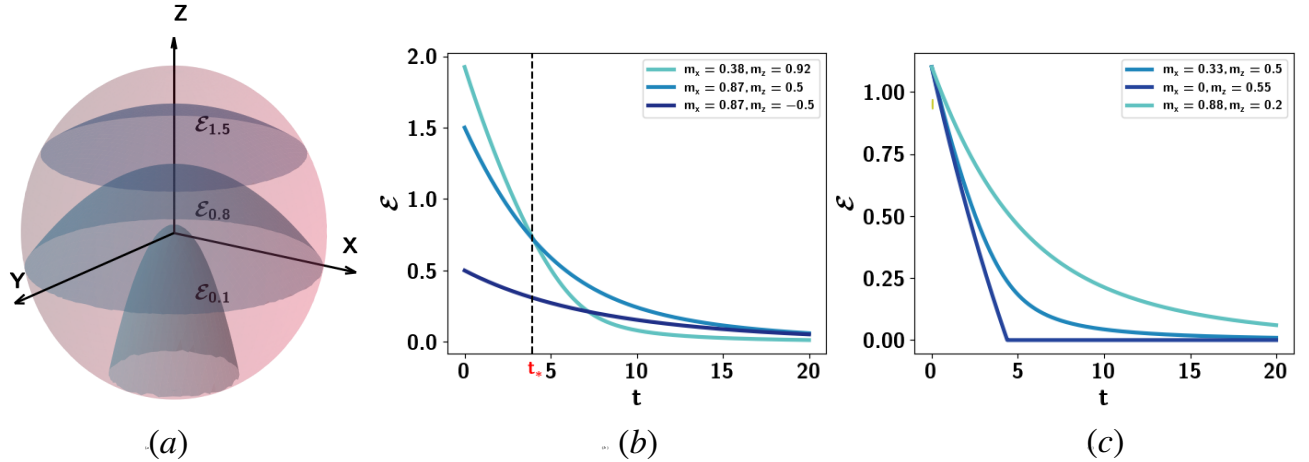


FIG. 1. **Ergotropy Mpemba crossing in a qubit system under ADC.** (a) Isoergotropic surfaces for different values of ergotropy are plotted on the Bloch sphere using Eq. (6). This surface never intersects and forms a paraboloid surface in the Bloch sphere (see cf. [74]). (b) Ergotropy (ordinate) against time (abscissa) for different initial ergotropy states. There are pairs of states that show ergotropy Mpemba crossings at $t = t_*$, which depend upon the state and the noise strengths. Also, there exist pairs of states that do not show crossings at any finite time. (c) Decay of ergotropy for isoergotropic states. There is no EMC if the initial state belongs to the isoergotropic surface and the state with highest m_z relaxes faster than the others. Other parameters of the systems are $T = 0$ and $\gamma_- = 0.1$.

dynamics exhibiting EMC if there exists a finite time, $t = t_*$, such that

$$\mathcal{E}_1(t_*^-) > \mathcal{E}_2(t_*^-) \xrightarrow{t=t_*} \mathcal{E}_1(t_*^+) < \mathcal{E}_2(t_*^+), \quad (4)$$

where t_*^\pm denote times immediately before and after t_* , respectively.

A. State-dependent condition for EMC under amplitude damping noise

Let us consider a single qubit Hamiltonian for a quantum battery,

$$H_B^{d=2} = h_z \sigma_z,$$

where h_z and σ_z denote the strength of the external magnetic field and σ_z is the Pauli operator respectively. To analyze the emergence of the Mpemba crossing, we prepare two different initial states, having two different sets of magnetization components along the three spatial directions, denoted as m_i ($i \in x, y, z$), given by

$$\rho^{d=2}(0) = \frac{1}{2} (\mathbb{I}_2 + m_x \sigma_x + m_y \sigma_y + m_z \sigma_z), \quad (5)$$

where \mathbb{I}_2 is the two-dimensional identity operator. The ergotropy, in this case, leads to

$$\mathcal{E}(\rho^{d=2}(0)) = h_z \left(m_z + \sqrt{m_x^2 + m_y^2 + m_z^2} \right). \quad (6)$$

The above quadratic dependence generates a paraboloid structure in the Bloch sphere when the left hand side is constant,

defining *isoergotropic* surfaces (all states on a given surface, which has the rotational symmetry about the z -axis, possess identical ergotropy), parametrized by the magnetization vector (see Fig. 1(a)). From now on, we set $h_z = 1$ which does not hamper results as h_z only scales the energy of the system.

When the system is coupled to a thermal bath at temperature $T = 0$, the ergotropy of the time-evolved state becomes

$$\begin{aligned} \mathcal{E}(t, m_x, m_y, m_z) = & e^{-\gamma_- t} \left[(1 - e^{\gamma_- t} + m_z) \right. \\ & \left. + \sqrt{(1 - e^{\gamma_- t} + m_z)^2 + e^{\gamma_- t} (m_x^2 + m_y^2)} \right], \end{aligned} \quad (7)$$

which depends on the initial state parameters and the environmental dissipation rate. We observe ergotropy Mpemba crossings at a finite time t_* , where an initially higher-ergotropy state dissipates ergotropy more rapidly than a state with lower initial ergotropy. At $t = t_*$, the corresponding ergotropy curves intersect, as shown in Fig. 1(b). This demonstrates that the EMC can occur in finite-dimensional systems, in close analogy with earlier observations in continuous-variable quantum batteries [67], although the phenomenon is not generic. Indeed, for other choices of initial states, no such crossing is observed, indicating that the emergence of EMC is highly sensitive to the initial state preparation (see Fig. 1(c)).

Motivated by these observations, a natural question arises: “*What conditions on the initial states lead to the occurrence of an EMC?*” More specifically, *is there an underlying structural relationship between pairs of initial states that provides a criterion for the occurrence of the EMC?* To address these

questions, we prove the following two lemmas.

Lemma 1. *For a pair of isoergotropic states, the state possessing a larger magnetization along the z direction (m_z) exhibits a faster decay of ergotropy compared to the state with smaller m_z .*

Proof. Without loss of generality, we restrict our attention to states lying in the xz -plane, i.e., we set $m_y = 0$, reducing Eq. (7) as

$$\mathcal{E}(t, m_x, m_z) = e^{-\gamma_- t} \left[(1 - e^{\gamma_- t} + m_z) + \sqrt{(1 - e^{\gamma_- t} + m_z)^2 + e^{\gamma_- t} m_x^2} \right]. \quad (8)$$

For isoergotropic states, the initial ergotropy satisfies

$$\mathcal{E}_0 \equiv \mathcal{E}(0, m_x, m_z) = m_z + \sqrt{m_x^2 + m_z^2}, \quad (9)$$

where \mathcal{E}_0 is a constant. Rearranging this expression, $m_x^2 = \mathcal{E}_0^2 - 2\mathcal{E}_0 m_z$, and substituting this into Eq. (8), we now prove that for a given t and γ_- , the ergotropy monotonically decreases with the increase of m_z on this surface. This is true for all values of t and valid γ_- . To do so, we compute

$$\begin{aligned} \frac{\partial \mathcal{E}(t, m_z)}{\partial m_z} &= e^{-\gamma_- t} \left[1 + \frac{2(1 - e^{\gamma_- t} + m_z) - 2e^{\gamma_- t} \mathcal{E}_0}{2\sqrt{(1 - e^{\gamma_- t} + m_z)^2 + e^{\gamma_- t} m_x^2}} \right] \\ &= e^{-\gamma_- t} \left[1 + \frac{e^{-\gamma_- t}(1 + m_z) - 1 - \mathcal{E}_0}{\sqrt{(e^{-\gamma_- t}(1 + m_z) - 1)^2 + e^{-\gamma_- t} m_x^2}} \right] \\ &\equiv e^{-\gamma_- t} \left[1 + \frac{A}{B} \right]. \end{aligned} \quad (10)$$

First, note that $A \equiv e^{-\gamma_- t}(1 + m_z) - 1 - \mathcal{E}_0 < 0$, which follows from the inequalities

$$\begin{aligned} e^{-\gamma_- t}(1 + m_z) &< 1 + m_z \\ \Rightarrow e^{-\gamma_- t}(1 + m_z) - 1 &< m_z < \mathcal{E}_0 \\ \Rightarrow e^{-\gamma_- t}(1 + m_z) - 1 - \mathcal{E}_0 &< 0 \\ \Rightarrow A &< 0, \end{aligned} \quad (11)$$

where we have used $m_z < m_z + \sqrt{m_x^2 + m_z^2} = \mathcal{E}_0$. Secondly,

$$\begin{aligned} A^2 - B^2 &= \mathcal{E}_0^2 - 2\mathcal{E}_0 m_z e^{-\gamma_- t} + 2\mathcal{E}_0(1 - e^{-\gamma_- t}) \\ &\quad - e^{-\gamma_- t}(\mathcal{E}_0^2 - 2\mathcal{E}_0 m_z) \\ &= (1 - e^{-\gamma_- t})(\mathcal{E}_0^2 + 2\mathcal{E}_0) > 0, \end{aligned} \quad (12)$$

implying that $|\frac{A}{B}| > 1$. These two results together imply $\frac{\partial \mathcal{E}(t, m_z)}{\partial m_z} < 0$, demonstrating that in the xz -plane, the ergotropy of an isoergotropic state with a larger m_z relaxes faster than that of a state with a smaller m_z . Finally, because the amplitude damping channel is phase covariant, the time-evolved ergotropy is symmetric under rotations about the z -axis. Hence, the isoergotropic curve generates a rotationally symmetric surface in the Bloch sphere, and the above conclusion holds for all states on that surface. \square

Fig. 1(c) illustrates the relaxation dynamics of ergotropy for initial states lying on an isoergotropic surface (see also Ref. [74] and Appendix A of Ref. [78]). We now prove how the properties of initial states with identical initial ergotropy govern the subsequent ergotropy dynamics.

Lemma 2. *For two non-isoergotropic states with identical m_x , the state with the larger magnetization in the z -direction, m_z , exhibits a slower decay of ergotropy compared to the state with a smaller m_z .*

Proof. By fixing a value of $m_x = M_x$ in Eq. (8) and compute the derivative of the ergotropy with respect to m_z , we obtain

$$\begin{aligned} \frac{\partial \mathcal{E}(t, m_z)}{\partial m_z} &= e^{-\gamma_- t} \left[1 + \frac{1 - e^{\gamma_- t} + m_z}{\sqrt{(1 - e^{\gamma_- t} + m_z)^2 + e^{\gamma_- t} M_x^2}} \right] \\ &\equiv e^{-\gamma_- t} \left[1 + \frac{C}{D} \right] \end{aligned} \quad (13)$$

for which it can be shown that $|\frac{C}{D}| < 1$, since

$$|1 - e^{\gamma_- t} + m_z| < \sqrt{(1 - e^{\gamma_- t} + m_z)^2 + e^{\gamma_- t} M_x^2}.$$

Hence,

$$\frac{\partial \mathcal{E}(t, m_z)}{\partial m_z} > 0, \quad (14)$$

which shows that $\mathcal{E}(t, M_x, m_z)$ is a monotonically increasing function of m_z , when m_x is taken to be fixed. Hence the proof. \square

We are now ready to provide the conditions under which two initial states exhibit no Mpemba crossing in terms of their coherence.

Theorem 1. *For an amplitude damping channel, two arbitrary initial states ρ_1 and ρ_2 with initial ergotropies $\mathcal{E}_1 \geq \mathcal{E}_2$, do not exhibit the ergotropic Mpemba crossing if their coherence satisfy*

$$\mathcal{C}(\rho_1) \geq \mathcal{C}(\rho_2),$$

where $\mathcal{C}(\cdot)$ is the l_1 -norm of coherence in the energy eigenbasis of the battery Hamiltonian.

Proof. The proof follows from Lemmas 1 and 2, which together identify the surface of the spherocylinder and rely on the rotational symmetry of ergotropy about the z -axis under amplitude damping dynamics.

Let ρ_1 lie in the xz -plane with magnetization vector $\vec{m}_1 = (m_{x_1}, 0, m_{z_1})$ and initial ergotropy \mathcal{E}_1 , and similarly, the magnetization vector of ρ_2 with initial ergotropy \mathcal{E}_2 be $\vec{m}_2 = (m_{x_2}, 0, m_{z_2})$ with $|m_{x_2}| < |m_{x_1}|$. Here $\mathcal{E}_1 > \mathcal{E}_2$ (see Fig. 2(a)). To show that $\mathcal{E}_1(t) > \mathcal{E}_2(t)$ for all $t > 0$, consider a third state ρ_c which have same m_x value as ρ_2 lying on the isoergotropic curve corresponding to \mathcal{E}_1 . Thus, ρ_c has the same ergotropy as ρ_1 , and its magnetization vector is $\vec{m}_c = (m_{x_2}, 0, m_{z_c})$ with $m_{z_c} > m_{z_1}, m_{z_2}$. From Lemma 1, we obtain $\mathcal{E}_1(t) > \mathcal{E}_c(t)$, since both states lie on the same isoergotropic curve and ρ_c has the larger m_{z_c} value than m_{z_1} .

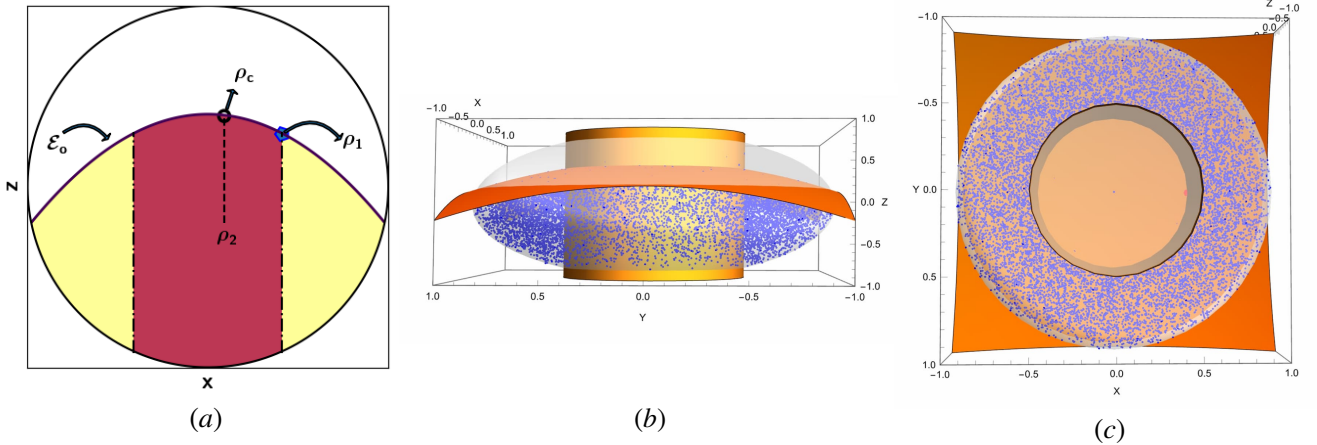


FIG. 2. **No EMC region for ADC channel.** (a) The non-EMC region is plotted in the xz -plane for a corresponding fixed state ρ_1 . The no-EMC region is denoted by the colored space bounded by the red lines and \mathcal{E}_o denotes the isoergotropic line in the xz -plane. (b) and (c) Side and down views of the EMC region where the dots in the sphere are the states that show EMC with a fixed state ρ_1 with ergotropy \mathcal{E}_o . Other parameters of the systems are $h_z = 1$, $T = 0$ and $\gamma_- = 0.01$.

Similarly, Lemma 2 implies $\mathcal{E}_1(t) > \mathcal{E}_c(t) > \mathcal{E}_2(t) \Rightarrow \mathcal{E}_1(t) > \mathcal{E}_2(t)$. Combining them, we get

$$\mathcal{E}_1(t) > \mathcal{E}_c(t) > \mathcal{E}_2(t) \Rightarrow \mathcal{E}_1(t) > \mathcal{E}_2(t). \quad (15)$$

Since ρ_2 is arbitrary within the region satisfying $\mathcal{E}_1 > \mathcal{E}_2$ and $|m_{x_2}| < |m_{x_1}|$, the set of such states forms a region, denoted by \mathcal{R}_{NE} in the xz -plane (see the darker region of Fig. 2(a)). Therefore,

$$\mathcal{E}_1(t) > \mathcal{E}_2(t) \quad \forall \rho_2 \in \mathcal{R}_{NE}. \quad (16)$$

Since the ADC is phase covariant, the ergotropy remains invariant under rotations about the z -axis. Rotating the region \mathcal{R}_{NE} forms a three-dimensional volume \mathcal{V}_{NE} in the Bloch sphere, which has the geometry of a spherocylinder (see Fig. 2(b) and (c)). Therefore, no Mpemba crossing occurs for any state ρ_2 within this region. Precisely, all states ρ_2 that lie inside the spherocylinder are characterized by a transverse distance from the z -axis given by $\sqrt{m_{x_2}^2 + m_{y_2}^2}$, which is bounded above by the corresponding distance $\sqrt{m_{x_1}^2 + m_{y_1}^2}$ associated with ρ_1 . This relation can be expressed as

$$\begin{aligned} \sqrt{m_{x_2}^2 + m_{y_2}^2} &\leq \sqrt{m_{x_1}^2 + m_{y_1}^2} \\ \Rightarrow \mathcal{C}(\rho_2) &\leq \mathcal{C}(\rho_1), \end{aligned} \quad (17)$$

where, in the last step, we have used the fact that the l_1 -norm of coherence of a qubit in the σ_z basis is given by $\sqrt{m_x^2 + m_y^2}$. \square

EMC region in terms of initial state parameters. The preceding analysis characterizes only the region in which the

EMC is absent and does not explicitly identify the set of states that *do* exhibit ergotropic Mpemba crossings with a fixed reference state, ρ_1 which we will now illustrate.

Let us now analyze the asymptotic behavior of the ergotropy in the long-time limit, $t \rightarrow \infty$, in Eq. (8) leading to

$$\begin{aligned} \mathcal{E}(t, m_x, m_z) &\simeq e^{-\gamma_- t} (1 + m_z - e^{\gamma_- t}) + \sqrt{1 + e^{-\gamma_- t} (m_x^2 - 2(1 + m_z))} \\ &\simeq e^{-\gamma_- t} (1 + m_z) + \frac{1}{2} e^{-\gamma_- t} (m_x^2 - 2(1 + m_z)) \\ &= \frac{1}{2} m_x^2 e^{-\gamma_- t} \end{aligned} \quad (18)$$

This shows that, at long times, the ergotropy decays exponentially and depends solely on the transverse magnetization m_x . Consider a state ρ_2 lying outside the spherocylinder but under the isoergotropic surface, corresponding to the reference state ρ_1 . If $\mathcal{C}(\rho_2) > \mathcal{C}(\rho_1)$, $|m_{x_2}| > |m_{x_1}|$, it implies that at sufficiently large times, the ergotropy of $\rho_2(t)$ exceeds that of $\rho_1(t)$. However, by assumption, the initial ordering satisfies $\mathcal{E}_1 > \mathcal{E}_2$ and hence, we have $\mathcal{E}_1 > \mathcal{E}_2 \rightarrow \mathcal{E}_1(t \rightarrow \infty) < \mathcal{E}_2(t \rightarrow \infty)$, which necessarily implies the existence of a finite crossing time $t = t_*$. Therefore, for $d = 2$, the l_1 -norm of coherence constitutes a criterion for the occurrence of EMC.

Note. Although the entire above analysis is discussed at the zero-temperature limit $T = 0$, the corresponding Mpemba crossing region remains unchanged, and the result can be straightforwardly generalized to finite temperatures $T \neq 0$, i.e., for gADC.

It is straightforward to observe that **Theorem 1** applies to all states irrespective of their purity. For arbitrary initially pure states given by the form $|\psi(\theta, \phi)\rangle = \cos \frac{\theta}{2} |0\rangle + e^{i\phi} \sin \frac{\theta}{2} |1\rangle$, one can derive an explicit condition with respect

to the state parameters when ergotropic Mpemba crossings is absent.

Corollary 1. *Two arbitrary pure states $|\psi_1(\theta_1, \phi_1)\rangle$ and $|\psi_2(\theta_2, \phi_2)\rangle$ when disturbed by gADC cannot exhibit the EMC when $\theta_1 + \theta_2 \geq \pi$.*

Proof. If ρ_1 lies on the surface of the Bloch sphere, it represents a pure state and can be written as $|\psi(\theta_1, \phi_1)\rangle$ (see Fig. 2(a)). Let the pure state which also lies on the Bloch sphere surface, and is connected to $|\psi(\theta_1, \phi_1)\rangle$ along a vertical line be denoted as $|\psi(\theta_2, \phi_2)\rangle$. These two states form the corners of the region \mathcal{R}_{NE} . Further, $|\psi(\theta_1, \phi_1)\rangle$ and $|\psi(\theta_2, \phi_2)\rangle$ are mirror images of each other with respect to the plane $z = 0$. This geometric symmetry directly implies $\theta_1 + \theta_2 \geq \pi$. \square

Mpemba crossing time. Let us now determine the precise time at which the ergotropy curves cross, i.e., the Mpemba crossing time, t_* . In general, it is hard to calculate for any two arbitrary qubit. Here, we find out t_* for any two arbitrary pure states, which is given as

$$t^* = \frac{1}{a\gamma} \ln \left(4 \left[\frac{a(1 + \cos \theta_1 \cos \theta_2) + (\cos \theta_1 + \cos \theta_2)}{(\cos \theta_1 + \cos \theta_2)(4 + a(\cos \theta_1 + \cos \theta_2))} \right] \right), \quad (19)$$

where $a = 1 + 2n$ with $\gamma_+ = \gamma n$, $\gamma_- = \gamma(1 + n)$ and $n = \frac{1}{e^{2h_Z\beta} - 1}$ is the mean number of bosons in the thermal state of temperature T . One can immediately check that t_* diverges when $\theta_1 + \theta_2 \geq \pi$. Therefore, this condition provides a sharp criterion for identifying the class of pure states that never exhibit an EMC. Conversely, whenever the crossing occurs, Eq. (19) yields the exact value of the crossing time. Note that the ergotropic profiles of ρ_1 and ρ_2 with time can indicate the strength of the ergotropic Mpemba. To quantify this, we consider the definition of “Mpemba parameter” [79] in the context of ergotropy (see Appendix C).

B. Constraints on initial States for EMC against an anisotropic Pauli channel

Let us now move to the scenario when the battery is exposed to the anisotropic Pauli channel. Unlike ADC, we obtain a trade-off relation between the dissipation strength, initial energy and coherence of the initial states in order to obtain EMC in the following. Let $E_{1(2)}$ be the energy of the state $\rho_{1(2)}$.

Theorem 2. *For an anisotropic Pauli channel, the occurrence of ergotropic Mpemba crossings between two states ρ_1 and ρ_2 with $\mathcal{E}_1 > \mathcal{E}_2$ and $m_z > 0$, depends on the relative strengths of the transverse and longitudinal noise rates – if $\gamma_\perp < \gamma_z$, an EMC occurs when $E_1 < E_2$ while in the region with $\gamma_\perp > \gamma_z$, EMC can be observed, provided $\mathcal{C}(\rho_1) < \mathcal{C}(\rho_2)$.*

Proof. For the detailed proof, see Appendix D. \square

Physically, the dependency of the EMC under the change of noise strength can be understood from the action of the noise on the states. The anisotropic noise squeezes the Bloch sphere

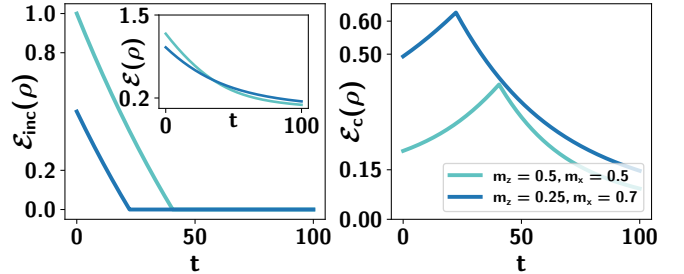


FIG. 3. Incoherent and coherent ergotropies against time, t for ADC. (a) Incoherent ergotropy, $\mathcal{E}_{inc}(\rho)$ (ordinate) vs time, t . The incoherent ergotropy decreases exponentially, which does not show any crossings. (b) Coherent ergotropy, $\mathcal{E}_c(\rho)$ against t . It increases upto a certain time, t_c , and then decreases sharply. This increasing behavior makes the delay in total ergotropy, leading to the ergotropic Mpemba crossing. Other parameters are same as in Fig. 2.

along the xy -plane while the transverse noise is a dephasing channel, squeezes the Bloch sphere along the z -axis. While $\gamma_\perp > \gamma_z$, the anisotropic part dominates, it tries to destroy the coherence of the state. Hence, the coherence plays a pivotal role for the occurrence of ergotropic Mpemba crossing while in $\gamma_\perp < \gamma_z$, the coherence decays faster and the system squeezes along the z -axis, which depends upon m_z , only, in turn, depends on the initial energy of the systems.

III. INCOHERENT AND COHERENT ERGOTROPY IN ERGOTRIC MPEMBA EFFECT

To gain insight into the physical origin of the EMC, we analyze the finer structure of ergotropy by decomposing it into its coherent and incoherent contributions [45]. The incoherent ergotropy quantifies the maximum extractable work achievable without altering the coherence of the density matrix, whereas the coherent ergotropy accounts for the additional work that can be extracted by modifying the coherence of the state. Accordingly, the total ergotropy of a quantum state ρ can be written as

$$\mathcal{E}(\rho) = \mathcal{E}_{inc}(\rho) + \mathcal{E}_c(\rho). \quad (20)$$

For $T \neq 0$, gADC modifies the population of the energy eigenstates, i.e., the population of the excited state decreases while the same for the ground state increases. At long times, the system approaches a thermal state in which the ground state is more populated than the excited state. Consequently, there exists a finite time $t = t_s$ at which the ground state population becomes higher than the excited state, causing the incoherent ergotropy to vanish. This behavior can be understood from the analytical form of the incoherent ergotropy dynamics, which is given as

$$\mathcal{E}_{inc} = 2\theta(t_s - t) \frac{1}{1 + 2n} [e^{-(1+2n)\gamma} (1 + m_z(1 + 2n)) - 1], \quad (21)$$

where $\theta(\cdot)$ is the Heaviside step function, defined as $\theta(t) = 1$ for $t > 0$ and $\theta(t) = 0$ for $t < 0$, and correspondingly, the

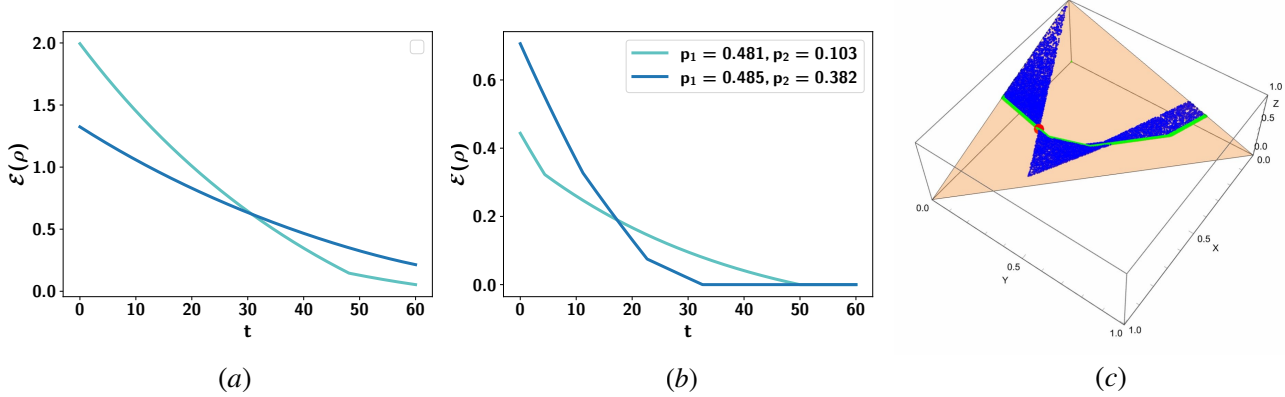


FIG. 4. **EMC for a qutrit battery under ADC channel.** (a) Ergotropy dynamics against time t for two arbitrary pure states to highlight that EMC can be observed in higher-dimensional system. (b) $\mathcal{E}(\rho)$ vs t for two pairs of diagonal initial states, $\rho^{d=3}(0) = p_1 |2\rangle\langle 2| + p_2 |1\rangle\langle 1| + (1 - p_1 - p_2) |0\rangle\langle 0|$. Note that unlike two-level quantum battery, the incoherent ergotropy alone can show the ergotropic Mpemba crossing. The set of state parameters chosen are $\{p_1 = 0.481, p_2 = 0.103\}$ (light solid line) and $\{p_1 = 0.485, p_2 = 0.382\}$ (dark solid line). (c) The EMC region of all the diagonal states are plotted for a fixed diagonal reference state (marked as solid circle). The (blue) dots are the states which show EMC with respect to the fixed state and the (green) solid line represents the isoergotropic surface.

time,

$$t_s = \frac{1}{(1 + 2n)\gamma} \ln(1 + m_z(1 + 2n)), \quad (22)$$

after which the incoherent ergotropy vanishes. It follows immediately that \mathcal{E}_{inc} decays exponentially in time and depends only on the initial population imbalance m_z . At early times, the coherent contribution to ergotropy may increase, indicating a transient generation of coherent ergotropy. After a characteristic time, the coherent ergotropy begins to decay and eventually vanishes (see Fig. 3(b)). This temporary buildup of coherent ergotropy effectively delays the relaxation process, causing the total ergotropy to approach its steady-state value more slowly.

More specifically, we find that for two-dimensional systems, the incoherent ergotropy alone cannot give rise to ergotropic Mpemba crossings (see Fig. 3(a)). In contrast, the coherent contribution exhibits a qualitatively distinct and non-trivial dynamical behavior; an exchange in relaxation behavior occurs in which the coherent ergotropy relaxes more slowly, even though the incoherent part decays faster (see Fig. 3(a)). Consequently, for an EMC to occur, the coherent and incoherent contributions to ergotropy must be ordered differently for the two initial states ρ_1 and ρ_2 . This condition thus provides a criterion for the observation of EMC.

Beyond the generalized amplitude damping channel, a similar qualitative behavior is also observed for the anisotropic Pauli channel (see Appendix D). These analyses indicate that the emergence of the EMC is driven by the interplay between coherent and incoherent ergotropies. However, we will also show that such an argument does not hold when the dimension of the battery increases.

IV. QUTRIT SYSTEM ERGOTROPIC MPEMBA EFFECT

So far, we have restricted our analysis to qubit systems in which the geometric simplicity of the Bloch sphere plays a crucial role in enabling an analytical characterization of the EMC. Extending such an analysis to arbitrary higher dimensions d is, however, significantly more challenging. As a first step towards understanding higher-dimensional quantum batteries, we now consider a three-level ($d = 3$) system described by the Hamiltonian $H_B^{d=3} = h_z S_z$, where S_z is the generalized Pauli operator along the z -direction in three dimensions, and h_z denotes the strength of the external magnetic field. An arbitrary initial state in this three-dimensional Hilbert space can be written in the form

$$\rho^{d=3}(0) = \frac{1}{3} \left(\mathbb{I}_3 + \sum_{i=1}^8 r_i \hat{\Gamma}_i \right), \quad (23)$$

where $r_i = \text{Tr}[\rho^{d=3}(0) \hat{\Gamma}_i]$ with $\hat{\Gamma}_i$ being the Gell–Mann matrices, forming a basis for the Lie algebra SU(3) and satisfying $\text{Tr}[\hat{\Gamma}_i \hat{\Gamma}_j] = 2\delta_{ij}$.

After preparing the initial state, the system is subjected to an amplitude damping channel, and the corresponding Lindblad operators governing the dynamics are $L_j = |0\rangle\langle 1|, |0\rangle\langle 2|, |1\rangle\langle 2|$, where $\{|0\rangle, |1\rangle, |2\rangle\}$ represents the set of energy eigenstates of the battery Hamiltonian, ordered according to increasing energy, and γ is the associated (time-independent) decay rate for all the transitions. As in the qubit case, the environment induces spontaneous decay from the excited states toward the ground state. Consequently, the ground

state of $H_B^{d=3}$ is the unique steady state of the dynamics, and the ergotropy decays to zero in the long-time limit. Such maps can be cast into a block-diagonal form $\mathcal{L}_p \oplus \mathcal{L}_c$, where \mathcal{L}_p denotes the population block and \mathcal{L}_c as the coherence block (cf. Ref. [11]). It indicates that the population and coherence dynamics are independent of each other.

We find that like in the qubit case, an ergotropic Mpemba crossing in qutrit system can also be observed (see Fig. 4(a)), confirming the phenomena in higher-dimensional systems. In Fig. 4(a), we show that EMC is observed for two arbitrary pure states and there is a critical time t_* when the EMC is observed. However, the analysis for the whole state space in the case of qutrits is not analytically tractable. Hence, by considering all qutrit initial states with diagonal density matrices of the given form, $\rho^{d=3}(0) = p_1 |2\rangle\langle 2| + p_2 |1\rangle\langle 1| + (1 - p_1 - p_2) |0\rangle\langle 0|$, (where $0 \leq p_1, p_2 \leq 1$), we are able to show the region of states that show EMC. In this case, the dynamics of the ergotropy can be visualized within a probability simplex, as illustrated in Fig. 4(c). Note that the state remains diagonal throughout the evolution, which leads to the ergotropy being purely incoherent, i.e., $\mathcal{E}_c = 0$ and $\mathcal{E}_{inc} \neq 0$. In this context, it is noteworthy that, in contrast to the qubit case, an *incoherent* ergotropic Mpemba crossing can occur in a qutrit system (see Fig. 4(b)). The presence of additional energy levels leads to distinct relaxation rates between different pairs of levels, which, in turn, delays the saturation of ergotropy during the dynamics. As a consequence, ergotropic Mpemba crossings arise in qutrits, with their occurrence determined by the initial population distribution among the energy levels.

Ordering of probabilities	Ergotropy
$p_1 < p_2 < p_3$	0
$p_1 < p_3 < p_2$	$2p_2 + p_1 - 1$
$p_2 < p_1 < p_3$	$p_1 - p_2$
$p_2 < p_3 < p_1$	$3p_1 - 1$
$p_3 < p_1 < p_2$	$3(p_1 + p_2) - 2$
$p_3 < p_2 < p_1$	$4p_1 + 2p_2 - 2$

TABLE I. Ergotropy for different arrangements of populations in a diagonal qutrit states is presented where $p_3 = 1 - p_1 - p_2$.

We find that, analogous to the qubit case, isoergotropic surfaces play a crucial role in identifying the no-EMC (\mathcal{R}_{NE}) region within the probability simplex. In particular, the isoergotropic surfaces form the boundary of the region where EMCs occur. For diagonal qutrit states, there are six distinct ways to order the level populations in increasing order and each ordering corresponds to a different functional form of the ergotropy in terms of the independent probabilities p_1 and p_2 , as summarized in Table I. A point lies on a given isoergotropic surface only if it satisfies both the left- and right-hand conditions of the corresponding expressions listed in Table I. We numerically identify a subset of states represented by the dark-shaded region in Fig. 4(c) that exhibit EMC with a fixed

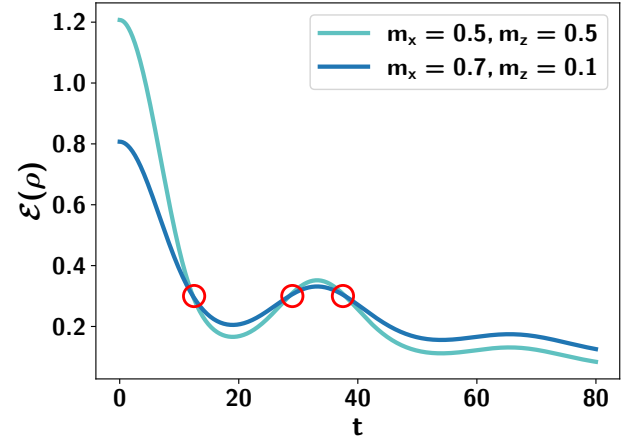


FIG. 5. **Dynamics of Ergotropy under non-Markovian noise.** For a qubit battery, the EMC can be observed under non-Markovian noisy channel. Interestingly, an odd number of crossings is observed in the transient regime, and these curves never intersect after a certain time, referred to as *quasiergotropic* Mpemba effect [30]. All other system parameters are $\lambda = 0.03$, $\Delta = 0.13$ and $\gamma = 0.3$.

reference state (marked as a solid circle). Notably, as in the qubit case, the boundary of this region is formed by isoergotropic states, indicated by the green curve. This observation highlights that a detailed understanding of the isoergotropic surfaces is essential for characterizing the EMC region associated with a given reference state.

V. NON-MARKOVIAN ERGOTROPIC MPEMBA EFFECT

Relaxing the assumption of Markovian dynamics, under which ergotropy decays monotonically in time, we now address the following question: *"Can the ergotropic Mpemba crossing persist in the non-Markovian regime, where information backflow from the environment to the system leads to memory effects and induces collapse and revival of ergotropy?"* To address this, let us consider the battery Hamiltonian of the system (H_B), environment (H_E) and system-environment interaction (H_{BE}^{int}), given by

$$H = \underbrace{h_z \sigma_z}_{H_B} + \underbrace{\sum_k \omega_k b_k^\dagger b_k}_{H_E} + \underbrace{\sum_k (g_k \sigma_+ b_k + g_k^* \sigma_- b_k^\dagger)}_{H_{BE}^{\text{int}}}, \quad (24)$$

where the bath consists of harmonic oscillators having frequency ω_k of the k -th mode, $b_k(b_k^\dagger)$ is the annihilation (creation) operator for the k -th mode of the bath, and the coupling strength between the system and the mode k of the bath is denoted as g_k . In the interaction picture, the interaction Hamiltonian reads as $H^{\text{int}} = \sum_k g_k \sigma_+ b_k e^{i(2h_z - \omega_k)t} + \text{h.c.}$. We consider the bath to have Lorentzian spectral density, given by $J(\omega) = \frac{1}{2\pi} \frac{\gamma \lambda^2}{(2h_z - \Delta - \omega)^2 + \lambda^2}$, where λ is the width of the spectrum, γ is the effective coupling and Δ is the detuning of the

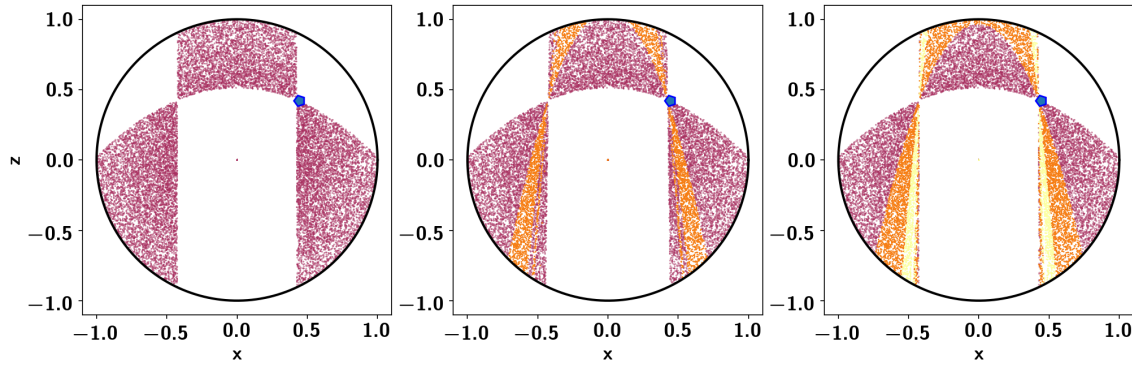


FIG. 6. **Ergotropic Mpemba crossing regions are plotted in xz -plane with respect to a fixed state ρ_1 (given by blue dots).** Different shades of color represent the number of crossings in the transient regime between the fixed state and the states in the EMC region. The red dots represent the states with which the state corresponding to the reference state show a single EMC, the orange (lighter shade) dots correspond to the states for which three EMCs are observed while the yellowish (more lighter dots) dots are states with five EMCs. The non-Markovianity of the evolution is increased from left to right, specifically the parameters are chosen as (a) $(\gamma, \lambda) = (0.05, 0.2)$ (b) $(\gamma, \lambda) = (0.3, 0.03)$ and (c) $(\gamma, \lambda) = (1.0, 0.03)$. Here $\Delta = 0.1$.

system and the central frequency of the bath. It is known that for $\gamma/\lambda \ll 1$, the dynamics is Markovian, and for $\gamma/\lambda \gg 1$, it is non-Markovian [62, 80].

Initializing the system in an arbitrary pure state and the environment in the vacuum state of the bath, i.e., $|\psi(0)\rangle = (\alpha|0\rangle + \beta|1\rangle) \otimes |0\rangle_E$, where α, β are complex numbers with $|\alpha|^2 + |\beta|^2 = 1$. The evolution of the total system can be obtained analytically as

$$|\psi(t)\rangle = \alpha\nu(t)|0\rangle \otimes |0\rangle_E + \sum_k \eta_k(t)|1\rangle \otimes |1_k\rangle_E + \beta|1\rangle \otimes |0\rangle_E, \quad (25)$$

with $\nu(t) = e^{-\frac{\lambda t}{2}} \left(\cosh\left(\frac{\zeta t}{2}\right) + \frac{\lambda - i\Delta}{\zeta} \sinh\left(\frac{\zeta t}{2}\right) \right)$ where $\zeta^2 = (\lambda - i\Delta)^2 - 2\gamma\lambda$. After tracing out the bath, the state of the battery at arbitrary time becomes

$$\rho(t) = \begin{pmatrix} |\alpha\nu|^2 & (\alpha\nu)\beta \\ (\alpha\nu)^*\beta^* & 1 - |\alpha\nu|^2 \end{pmatrix}. \quad (26)$$

Instead of pure state of the system, if one considers a mixed initial state, by using linearity of the channel, the evolved state of the system can be written as

$$\rho(t) = \lambda_+ \rho_+(t) + \lambda_- \rho_-(t), \quad (27)$$

where $\lambda_{\pm} = \frac{1}{2}(1 \pm |\vec{m}|)$ are the eigenvalues of the initial state, $\rho_0 = \lambda_+ |\psi_+\rangle \langle \psi_+| + \lambda_- |\psi_-\rangle \langle \psi_-|$, with $|\psi_{\pm}\rangle = \cos\frac{\theta}{2}|0\rangle \pm e^{i\phi} \sin\frac{\theta}{2}|1\rangle$ being the eigenstates of the initial state. Considering any arbitrary mixed state, $|\vec{m}| = \sqrt{m_x^2 + m_y^2 + m_z^2}$ and $\rho_{\pm}(t)$ is the evolved state when the

initial state is $|\psi_{\pm}\rangle$ respectively. The ergotropy of the battery starting from any arbitrary mixed state can be computed as

$$\mathcal{E} = \frac{(|\nu|^2(1 + |\vec{m}| \cos \theta) - 1)}{\sqrt{(|\nu|^2(1 + |\vec{m}| \cos \theta) - 1)^2 + |\vec{m}|^2 \sin^2 \theta |\nu|^2}}, \quad (28)$$

which turns out to be independent of the phase, ϕ , due to the phase covariant nature of the dynamics. Analyzing the behavior of \mathcal{E} , two regimes in the non-Markovian evolution emerge, namely (i) the *transient* and (ii) the *steady state*. In the *transient* regime (see Fig. 5), an oscillatory behavior of the ergotropy, a signature of non-Markovianity, can be observed, while at the long-time limit, the oscillations become less pronounced. Interestingly, we find that unlike Markovian case, there are multiple crossing points in the transient time (cf. [30]) although a specific time $t = t_m$ exists at which the final crossing occurs, after which the two curves never intersect again, named the *quasiergotropic Mpemba effect*.

Even vs odd crossing. Like the Markovian case, we can also identify the region in the Bloch sphere of the initial states that exhibit Mpemba crossings in the non-Markovian evolution as well. In order to identify this, we again use the phase covariance of the ergotropy and hence, it is sufficient to consider the ergotropy in the xz -plane. We probe into the large-time behavior of ergotropy in the non-Markovian evolution, which is

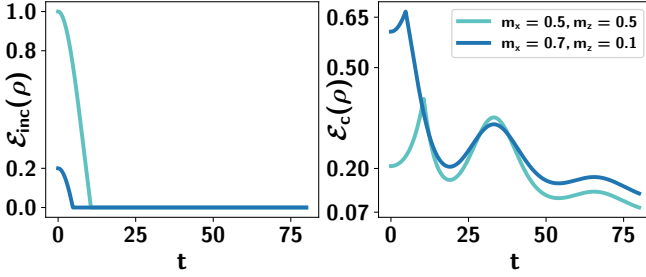


FIG. 7. **Dynamical profile of incoherent and coherent ergotropies under non-Markovian channel.** (a) Incoherent and (b) coherent ergotropy (ordinate) against time, t (abscissa). Other system parameters are same as in Fig. 5.

given as

$$\begin{aligned} \mathcal{E} \sim & \left(|\nu|^2 (1 + |\vec{m}| \cos \theta) - 1 \right) + 1 - |\nu|^2 (1 + |\vec{m}| \cos \theta) \\ & + \frac{|\nu|^2}{2} |\vec{m}|^2 \sin^2 \theta \\ \Rightarrow \mathcal{E} \sim & \frac{|\nu|^2}{2} m_x^2, \end{aligned} \quad (29)$$

where we have considered t to be large. Note that the ergotropy depends upon ν and the initial magnetization, m_x . In turn, the ergotropy behavior depends upon the l_1 -coherence of the state as m_x^2 is the coherence in the xz -plane. From eq. (29), it is clear that at large time, $m_{x_1}^2 > m_{x_2}^2$ implies that $\mathcal{E}(\rho_1(t \rightarrow \infty)) \geq \mathcal{E}(\rho_2(t \rightarrow \infty))$ which implies that they cross each other an even number of times. On the other hand, $m_{x_1}^2 \leq m_{x_2}^2$, there is at least an odd number of crossings that emerged as EMC in non-Markovian evolution (see Fig. 5). Also, interestingly, we determine the region of states that shows different odd numbers of crossings in the transient regime (see Fig. 6). In Fig. 6, we illustrate the number of EMC for different initial states while keeping one reference state fixed. Interestingly, the number of states displaying a single crossing increases with the degree of non-Markovianity, as depicted in Fig. 6(a). In contrast, the population of states exhibiting multiple crossings grows with increasing non-Markovianity, as indicated by the variation in color intensity in Fig. 6(b) and (c).

Interestingly, we find out that there is no even number of crossings. In order to prove that there is no even number of crossings possible, we use the following two lemmas which are given as follows:

Lemma 3. *For two isoergotropic states, the ergotropy of the state with a larger magnetization along the z -direction decays faster than that of the state with a smaller m_z for non-Markovian amplitude damping channel.*

Lemma 4. *For two non-isoergotropic states with identical m_x , the ergotropy of the state with a larger m_z decays more slowly than that of the state with a smaller m_z .*

For the proof of the Lemmas, see Appendix E 1.

Analogous to **Theorem 1**, Lemmas 3 and 4 together establish the existence of a region \mathcal{R}_{NE} in the xz plane of the Bloch sphere, consisting of states that do not exhibit any ergotropic Mpemba crossings during the evolution. The presence of this

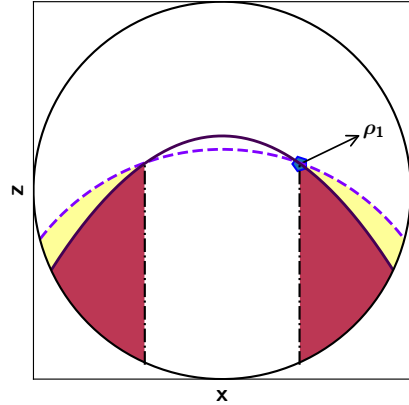


FIG. 8. **Comparison between the ergotropic Mpemba crossing and the state Mpemba effect for a qubit evolving in the xz -plane under ADC.** The solid curve denotes the isoergotropic line, while the dashed curve represents states that are equidistant from the steady state. The darker shaded region corresponds to states, exhibiting both EMC and the state Mpemba effect, whereas the lighter shaded region indicates states that display the state Mpemba effect without showing EMC. The remaining parameters are fixed as $T = 0$, $\gamma_- = 0.01$, and the reference state ρ_1 is chosen with $m_x = 0.4$ and $m_z = 0.15$.

region excludes the possibility of an even number of crossings in the non-Markovian regime.

Coherent and incoherent ergotropy in non-Markovian dynamics. As observed in the Markovian case, the coherent and incoherent contributions to the ergotropy, \mathcal{E}_c and \mathcal{E}_{inc} , display qualitatively similar roles in non-Markovian dynamics for qubits. The incoherent contribution decays rapidly, whereas the decay of the coherent ergotropy occurs over a longer timescale. During the transient regime, oscillatory behavior emerges as a signature of memory effects (see Fig. 7). Remarkably, in the non-Markovian dynamics, we observe an exchange of dominance between the coherent and incoherent contributions to ergotropy, which leads to the emergence of the *quasi-ergotropic Mpemba effect*. In this regime, a trade-off between \mathcal{E}_c and \mathcal{E}_{inc} is required for the appearance of Mpemba crossings. These findings indicate that ergotropic Mpemba crossings arise from a combined and subtle interplay between the incoherent and coherent components of ergotropy.

VI. CONNECTION BETWEEN EMC AND STATE MPMEMBA EFFECT

It is well known that the dynamical behavior of a quantum state and that of its associated observables can differ significantly; for instance, cloning a quantum state is fundamentally distinct from cloning the expectation value of an operator. Motivated by the conjecture that Mpemba crossings may arise from properties of specific observables rather than from intrinsic features of the quantum state itself [71], we an-

alyze the relationship between trace-distance dynamics¹ and ergotropy. In order to perform the analysis, we keep the reference state, ρ_1 fixed for ergotropy and state evolution, i.e., we want to find out the region of state that show EMC and state Mpemba effect with a fixed reference state ρ_1 .

We begin by considering the gADC with initial states restricted to the xz -plane. In this setting, the set of states that are equidistant from the steady state is described by

$$\frac{\sqrt{m_x^2 + (1 + m_z)^2}}{4} = \kappa, \quad (30)$$

where κ is a constant. This relation defines a curve in the xz -plane (see the dashed curve in Fig. 8). The time-dependent trace distance from the steady state is given by

$$\mathcal{D}(t) = \frac{e^{-at\gamma} \sqrt{\frac{1}{4} + m_x^2 a^2 \frac{e^{a\gamma t}}{4} + \frac{am_z}{2} (1 + \frac{am_z}{2})}}{a}, \quad (31)$$

where $a = 1 + 2n$. To identify the region of states exhibiting the state Mpemba effect with a reference state ρ_1 , we analyze the long-time limit $t \rightarrow \infty$. In this regime, the trace distance with the steady state simplifies to $\mathcal{D}(t) \sim \frac{|m_x|}{2} e^{-\frac{t\gamma}{2}}$, revealing an exponential decay governed by the transverse magnetization $|m_x|$, which quantifies coherence in the xz -plane. Analogous to the behavior of ergotropy, two states satisfying $\mathcal{C}(\rho_1) < \mathcal{C}(\rho_2)$ exhibit the state Mpemba effect. Consequently, the region of states displaying the state Mpemba effect is bounded by the equidistance curve together with the coherence of the chosen reference state (as shown in Fig. 8).

A similar analysis can be carried out for the anisotropic Pauli channel. In this case, the set of states that share the same trace distance from the steady state is described by $\sqrt{\frac{m_x^2}{4} + \frac{m_z^2}{4}} = \kappa$, where κ is a constant. The time evolution of the trace distance is given by

$$\mathcal{D}(t) = e^{-2t(3\gamma_{\perp} + \gamma_z)} \sqrt{e^{8t\gamma} \frac{m_x^2}{4} + \frac{e^{4t(\gamma_{\perp} + \gamma_z)} m_z^2}{4}}. \quad (32)$$

In the long-time limit, when $\gamma_z > \gamma_{\perp}$, the decay of the trace distance is approximately $e^{-4\gamma t} \frac{|m_z|}{2}$, whereas for $\gamma_{\perp} > \gamma_z$, it behaves as $e^{-2t(\gamma_{\perp} + \gamma_z)} \frac{|m_x|}{2}$. Thus, both the initial energy (through m_z) and the coherence (through m_x) play a role in determining the occurrence of Mpemba crossings for states.

Qutrit system. For diagonal qutrit states evolving under the amplitude damping channel governed by Eq. (A1), the trace distance from the stationary state is given by $e^{-\gamma t}(p_1 + p_2)$, where p_1 and p_2 denote the initial populations of the excited levels and γ is the dissipation strength. Owing to its purely exponential dependence on time, no crossings occur in the trace distance dynamics for diagonal states. Consequently, diagonal states in the energy basis do not exhibit the state Mpemba

effect for any pair of initial states. Nevertheless, as shown in Fig. 4(b), ergotropic Mpemba crossings can still arise for such diagonal qutrit states.

For both noise models, we observe that in a qubit system, all states exhibiting ergotropic Mpemba crossings (EMC) also display the state Mpemba effect, although the converse is not generally true (as shown in Fig. 8). To examine whether this behavior persists in higher dimensions, we extend our analysis to qutrit systems. These findings demonstrate that Mpemba crossings may occur in the trace distance without corresponding ergotropic Mpemba crossings, and conversely, ergotropic Mpemba crossings may arise without state Mpemba crossings in systems with dimension greater than two. Hence, there is no universal one-to-one correspondence between the two phenomena; rather, any apparent correlation is strongly system-dependent.

VII. CONCLUSION

The quantum Mpemba effect is the quantum analogue of the classical Mpemba effect, wherein a system initially farther from equilibrium can relax to its equilibrium state faster than a system that is initially closer to equilibrium. Such counter-intuitive behavior is of practical interest in quantum technologies, as it can potentially be exploited to enhance the performance of quantum devices.

Motivated by the broader relevance of nonequilibrium relaxation phenomena, we investigated the ergotropic Mpemba effect in finite-dimensional quantum systems, with a particular focus on two- and three-level systems. Concentrating on ergotropic Mpemba crossings (EMC), defined as instances where two ergotropy curves intersect at least once during the dynamics, we derived a criterion for the occurrence of such crossings. Specifically, we showed that when the system is governed by a generalized amplitude damping channel (gADC), the occurrence of EMC is entirely dictated by the relative coherence of the initial states. This allows us to characterize the complete set of states that do not exhibit crossings with a fixed reference state and to show that this set forms a spherocylinder in state space, with the reference state lying on its surface. Beyond the gADC, we also established the conditions for EMC in the presence of an anisotropic Pauli channel and found that both coherence and energy jointly control the emergence of EMC. To elucidate the physical origin of ergotropic Mpemba crossings, we analyzed the coherent and incoherent contributions to ergotropy. In two-dimensional systems, we revealed that the incoherent ergotropy decays exponentially in time and does not exhibit Mpemba behavior, whereas the coherent ergotropy displays a transient increase followed by a rapid decay, indicating that the delayed relaxation of ergotropy is governed by the coherent contribution. In contrast, for three-level systems, we demonstrated that incoherent ergotropy alone can exhibit EMC due to the presence of multiple relaxation pathways between energy levels with different rates.

We further extended our analysis to non-Markovian dynamics, where we showed that, unlike the Markovian case,

¹ The trace distance between two quantum states ρ_1 and ρ_2 is defined as half of the trace norm of their difference, and is given by $\mathcal{D}(\rho_1, \rho_2) = \frac{1}{2} \text{Tr} \left[\sqrt{(\rho_1 - \rho_2)^{\dagger}(\rho_1 - \rho_2)} \right]$.

multiple ergotropic Mpemba crossings may occur. In particular, we proved that the total number of crossings is always odd. Further, we explored the relationship between ergotropic Mpemba crossings and the conventional state Mpemba effect. For two-dimensional systems, we observed that the presence of ergotropic Mpemba crossings implies the presence of state Mpemba crossings, although the converse need not hold. Our results provide criteria for identifying initial states that enable faster energy extraction in finite-dimensional systems, offering practical guidance for the realization and optimization of quantum batteries in laboratory settings.

ACKNOWLEDGMENTS

We acknowledge support from the project entitled “Technology Vertical - Quantum Communication” under the National Quantum Mission of the Department of Science and Technology (DST) (Sanction Order No. DST/QTC/NQM/QComm/2024/2 (G)). This research was carried out and financed within the framework of the second Swiss Contribution MAPS (Grant No. 230870).

Appendix A: Vectorization of GKSL master equation

Unlike unitary evolution, open-system dynamics are not invertible and instead form a semigroup. The evolution of the system is governed by the GKSL master equation, given by

$$\frac{d\rho}{dt} = -i[H_B, \rho] + \sum_k \gamma_k \left(L_k \rho L_k^\dagger - \frac{1}{2} \{L_k^\dagger L_k, \rho\} \right), \quad (\text{A1})$$

where ρ is the reduced density matrix of the system obtained after tracing out the environment and H_B is the Hamiltonian of the system. The operators L_k are the Lindblad jump operators that encode the action of the environment on the system, and γ_k denotes the corresponding decay rates determined by the system-environment coupling. Now, if the dynamics are governed by a GKSL master equation, i.e., the dynamics is Markovian, the corresponding quantum map is completely positive and divisible, and the time evolution can be written as

$$||\rho_t\rangle\rangle = e^{\mathcal{L}t} ||\rho_0\rangle\rangle, \quad (\text{A2})$$

where $||\rho_0\rangle\rangle$ is the vectorised initial state and \mathcal{L} denotes the Liouvillian superoperator. If the system consists of N number of qubits, then the Liouvillian superoperator becomes a $4^N \times 4^N$ matrix, consisting of complex eigenvalues, and generally, the left and right eigenvectors of the Liouvillian are not connected by complex conjugation. The Liouvillian operator can be obtained from Eq. (A1) which is given by

$$\mathcal{L} = -i[H_B \otimes \mathbb{I} - \mathbb{I} \otimes H_B^\text{T}] + \sum_j \frac{\gamma_j}{2} \left(2L_j \otimes L_j^* - L_j^\dagger L_j \otimes \mathbb{I} - \mathbb{I} \otimes L_j^T L_j^* \right) \quad (\text{A3})$$

Now, the solution of the evolved state is given as

$$||\rho_t\rangle\rangle = ||\rho_{ss}\rangle\rangle + \sum_{i \neq 1} c_i(0) e^{\lambda_i t} ||r_i\rangle\rangle, \quad (\text{A4})$$

where $||\rho_{ss}\rangle\rangle$ is the steady state and r_i are the right eigenmatrices of the matrix \mathcal{L} and $c_i(0) = \text{Tr}[l_i \rho_0]$ with l_i being the left eigenmatrices of \mathcal{L} . These eigenmatrices can be obtained by vectorization of the density matrix ρ [81].

Appendix B: The evolution of the system under gADC

1. Single qubit battery evolution

The evolution of the single qubit battery can be obtained via vectorization of the Lindbladian. In this case, the Lindbladian, \mathcal{L} becomes a matrix of dimension 4×4 , given by

$$\mathcal{L} = \begin{pmatrix} -\gamma_2 & 0 & 0 & \gamma_1 \\ 0 & -\frac{\gamma_1 + \gamma_2}{2} - 2\gamma_3 - 2ih_z & 0 & 0 \\ 0 & 0 & -\frac{\gamma_1 + \gamma_2}{2} - 2\gamma_3 + 2ih_z & 0 \\ \gamma_2 & 0 & 0 & -\gamma_1 \end{pmatrix}. \quad (\text{B1})$$

To find the evolved state, we need to find the right eigenvectors and the corresponding eigenvalues of \mathcal{L} are given as

$$\lambda_1 = 0, \quad \lambda_2 = -\gamma_1 - \gamma_2, \quad \lambda_{3,4} = \frac{1}{2}(-\gamma_1 - \gamma_2 - 4\gamma_3 \pm 4ih_z). \quad (\text{B2})$$

and the corresponding right eigenmatrices read

$$r_1 = \frac{1}{\gamma_1 + 1} \begin{pmatrix} \gamma_1 & 0 \\ \gamma_2 & 0 \\ 0 & 1 \end{pmatrix}, \quad r_2 = \begin{pmatrix} -1 & 0 \\ 0 & 1 \end{pmatrix}, \quad r_3 = \begin{pmatrix} 0 & 0 \\ 1 & 0 \end{pmatrix}, \quad r_4 = \begin{pmatrix} 0 & 1 \\ 0 & 0 \end{pmatrix}, \quad (\text{B3})$$

while the corresponding left eigenmatrices are

$$l_1 = \begin{pmatrix} 1 & 0 \\ 0 & 1 \end{pmatrix}, \quad l_2 = \frac{1}{\frac{\gamma_2}{\gamma_1} + 1} \begin{pmatrix} -\frac{\gamma_2}{\gamma_1} & 0 \\ 0 & 1 \end{pmatrix}, \quad l_3 = \begin{pmatrix} 0 & 1 \\ 0 & 0 \end{pmatrix}, \quad l_4 = \begin{pmatrix} 0 & 0 \\ 1 & 0 \end{pmatrix}. \quad (\text{B4})$$

Let the initial state be a pure state of the form $|\Psi(0)\rangle = \cos \frac{\theta}{2} |0\rangle + e^{i\phi} \sin \frac{\theta}{2} |1\rangle$ where, $|0\rangle$ ($|1\rangle$) is the ground (excited) state of the battery, H_B . The eigenvalues of the evolved state are given as

$$\lambda_- = \frac{1}{2} - \frac{1}{2as} \sqrt{(s-1-a \cos \theta)^2 + a^2 s e^{-4t\gamma_3} \sin^2 \theta}, \quad (\text{B5})$$

$$\lambda_+ = \frac{1}{2} + \frac{1}{2as} \sqrt{(s-1-a \cos \theta)^2 + a^2 s e^{-4t\gamma_3} \sin^2 \theta}, \quad (\text{B6})$$

where $\gamma_1 = \gamma n$, $\gamma_2 = \gamma(n+1)$, $a = 1 + 2n$ and $s = e^{at\gamma}$ with n being the bosonic occupation number. Now using the eigenvalues of the evolved state, the time-dependent ergotropy is given as

$$\mathcal{E}(t) = \frac{h_z(1-s+\cos \theta a)}{as} + \frac{h_z}{as} \sqrt{(s-1-a \cos \theta)^2 + a^2 s e^{-4t\gamma_3} \sin^2 \theta}. \quad (\text{B7})$$

2. Single qutrit battery evolution

To study the dynamics of the ergotropy of the three-level battery, we mainly consider the states with diagonal entry. The lindbladian superoperator is given by the following matrix:

$$\begin{pmatrix} -2\gamma & 0 & 0 & 0 & 0 & 0 & 0 & 0 & 0 \\ 0 & -ih_z - \frac{3\gamma}{2} & 0 & 0 & 0 & 0 & 0 & 0 & 0 \\ 0 & 0 & -2ih_z - \gamma & 0 & 0 & 0 & 0 & 0 & 0 \\ 0 & 0 & 0 & ih_z - \frac{3\gamma}{2} & 0 & 0 & 0 & 0 & 0 \\ \gamma & 0 & 0 & 0 & -\gamma & 0 & 0 & 0 & 0 \\ 0 & 0 & 0 & 0 & 0 & -ih_z - \frac{\gamma}{2} & 0 & 0 & 0 \\ 0 & 0 & 0 & 0 & 0 & 0 & 2ih_z - \gamma & 0 & 0 \\ 0 & 0 & 0 & 0 & 0 & 0 & 0 & ih_z - \frac{\gamma}{2} & 0 \\ \gamma & 0 & 0 & 0 & \gamma & 0 & 0 & 0 & 0 \end{pmatrix}, \quad (\text{B8})$$

where we have considered all the transition rates due to the environments are fixed to γ and the temperature of the bath to be $T = 0$. Owing to the block structure of the Lindblad generator, the state remains diagonal throughout the evolution given by

$$\rho(t) = R_1 - p_1 R_8 e^{-(2\gamma t)} - (p_1 + p_2) R_9 e^{-\gamma t}, \quad (\text{B9})$$

with

$$R_1 = \begin{pmatrix} 0 & 0 & 0 \\ 0 & 0 & 0 \\ 0 & 0 & 1 \end{pmatrix}, \quad R_8 = \begin{pmatrix} -1 & 0 & 0 \\ 0 & 1 & 0 \\ 0 & 0 & 0 \end{pmatrix}, \quad \text{and} \quad R_9 = \begin{pmatrix} 0 & 0 & 0 \\ 0 & -1 & 0 \\ 0 & 0 & 1 \end{pmatrix}. \quad (\text{B10})$$

Appendix C: Mpemba parameter for EMC

Going beyond a qualitative study, we quantify the EMC by addressing the natural question of how strong the effect

is when an EMC occurs. To quantify this strength, a quantity called ‘‘Mpemba parameter’’, analogous to that employed in the standard Mpemba effect [79] was introduced. It is defined

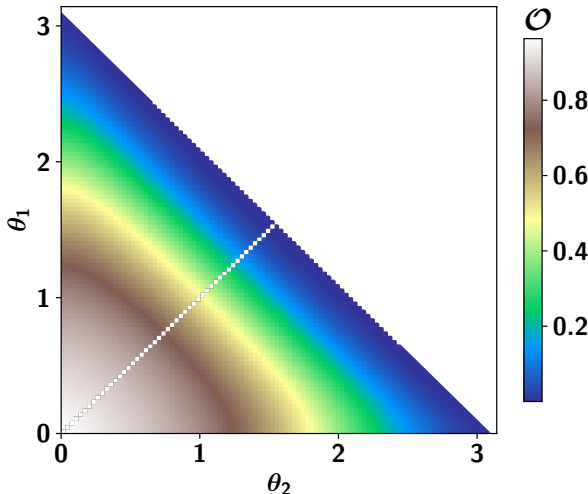


FIG. 9. Strength of ergotropic Mpemba crossing, quantified by \mathcal{O} is plotted in the (θ_1, θ_2) - plane for amplitude damping noise on a single qubit. No ergotropic mpemba crossing region for pure state can be found in the white region. Other parameters are $T = 0$ and $\gamma_- = 0.03$.

as

$$\mathcal{O} = \frac{\int_{\mathcal{E}_2 > \mathcal{E}_1} |\mathcal{E}_2(t) - \mathcal{E}_1(t)| dt}{\int_0^{t_f} |\mathcal{E}_2(t) - \mathcal{E}_1(t)| dt}, \quad (C1)$$

where $\mathcal{E}_1(t)$ and $\mathcal{E}_2(t)$ denote the ergotropies of the initially higher- and lower-ergotropy states, respectively. The quantity \mathcal{O} measures the fraction of the total enclosed area between the curves $\mathcal{E}_1(t)$ and $\mathcal{E}_2(t)$ that lies in the region where the initially lower-ergotropy state temporarily overtakes the higher-ergotropy one, i.e., prior to and after the ergotropic Mpemba crossing at $t = t_*$. Note that $0 \leq \mathcal{O} \leq 1$ and vanishes in the absence of any crossing. Values of \mathcal{O} close to zero correspond very Weak Mpemba effect, whereas values close to unity indicate Strong Mpemba effect. Thus, \mathcal{O} provides a useful quantitative indicator of the strenght of the ergotropic Mpemba effect.

In Fig. 9, we present the Mpemba parameter \mathcal{O} as a function of the state parameter θ , restricting our analysis to pure initial states. It is evident that when $\theta_1 + \theta_2 \geq \pi$, no Mpemba crossing occurs, as indicated by the white region in Fig. 9. This behavior is fully consistent with **Corollary 1**. Furthermore, the color gradient in the contour plot captures the variation of the Mpemba parameter.

For the single-qubit case, the slowest decaying modes (when $\gamma = 0.0$) are r_3 and r_4 , whose overlap with the initial pure state is given by $\sin \theta/2$. For the initial state $\theta = 0$, corresponding to the ground state $|0\rangle$, this overlap vanishes. Consequently, compared to a generic state on the Bloch sphere, the $|0\rangle$ state exhibits an exponential speedup in relaxation. As a result, a crossing in the relaxation dynamics is observed between the $|0\rangle$ state and any other state of the form given in Eq. (5) with arbitrary θ .

Appendix D: Anisotropic Pauli noise

In the case, when the battery is exposed to the anisotropic Pauli channel, we obtain an ergotropic Mpemba crossings (see Fig. 10 (a)), suggesting apart from Davis map, other quantum channel can showcase the EMC. We obtain a trade-off relationship between the dissipation strength and initial energy and coherence of the initial states. Unlike ADC, the initial energy of the state plays role in the occurrence of Mpemba crossings which give rise to the following theorem:

Theorem 2. *For an anisotropic Pauli channel, the occurrence of ergotropic Mpemba crossings between two states ρ_1 and ρ_2 with $\mathcal{E}_1 > \mathcal{E}_2$ and $m_z > 0$, depends on the relative strengths of the transverse and longitudinal noise rates, γ_\perp and γ_z . If $\gamma_\perp < \gamma_z$, an ergotropic Mpemba crossing occurs when $E_1 < E_2$, where $E_{1(2)}$ denotes the energy of the state $\rho_{1(2)}$. Conversely, if $\gamma_\perp > \gamma_z$, EMC occurs when $\mathcal{C}(\rho_1) < \mathcal{C}(\rho_2)$.*

Proof. To prove the theorem, we again exploit the phase-covariant nature of the anisotropic Pauli channel, which allows us to restrict the analysis to the evolution in the xz plane. The time-dependent ergotropy for an arbitrary initial state is given by

$$\mathcal{E}(t, m_z, m_x) = e^{-4\gamma_\perp t} \left[m_z + \sqrt{m_z^2 + e^{4t(\gamma_\perp - \gamma_z)} m_x^2} \right]. \quad (D1)$$

To identify the conditions for EMC, we analyze the long-time behavior of the ergotropy. In the case of $\gamma_\perp < \gamma_z$, the ergotropy at large t can be expressed as

$$\begin{aligned} \mathcal{E}(t) &\approx e^{-4\gamma_\perp t} \left[m_z + |m_z| \left(1 + \frac{e^{4t(\gamma_\perp - \gamma_z)} m_x^2}{2 m_z^2} \right) \right] \\ &\approx (m_z + |m_z|) e^{-4\gamma_\perp t} + \frac{e^{-4\gamma_z t}}{2} \frac{m_x^2}{|m_z|}. \end{aligned} \quad (D2)$$

Now in the case of $m_z > 0$, $\mathcal{E}(t \rightarrow \infty) \sim 2m_z e^{-4\gamma_\perp t}$ which tells that the decay of ergotropy depends solely on the initial magnetization along the z direction. For two initial states satisfying $\mathcal{E}_1(0) > \mathcal{E}_2(0)$, the structure of the isoergotropic curves in the xz plane implies $m_{z1} < m_{z2}$. Consequently, although ρ_1 initially possesses higher ergotropy, its ergotropy decays faster at long times, leading to

$$\mathcal{E}_1(t) < \mathcal{E}_2(t) \quad \text{for sufficiently large } t,$$

which guarantees the existence of an ergotropic Mpemba crossing at an earlier time. Since the energy of the initial state depends only on m_z , namely $E = \text{Tr}[\rho(0)H_B] = m_z/2$, the crossing condition can be expressed as

$$E_1 < E_2.$$

On the other hand, when $\gamma > \gamma_z$, in the long- time limit $t \rightarrow \infty$ we obtain

$$\mathcal{E}(t) \approx m_z e^{-4\gamma_\perp t} + e^{-2t(\gamma_\perp + \gamma_z)} |m_x| \quad (D3)$$

$$\begin{aligned} &+ \frac{1}{2} e^{-4\gamma_\perp t} e^{2t(\gamma_z - \gamma_\perp)} \frac{m_z^2}{|m_x|} \\ &\approx e^{-2t(\gamma + \gamma_z)} |m_x|. \end{aligned} \quad (D4)$$

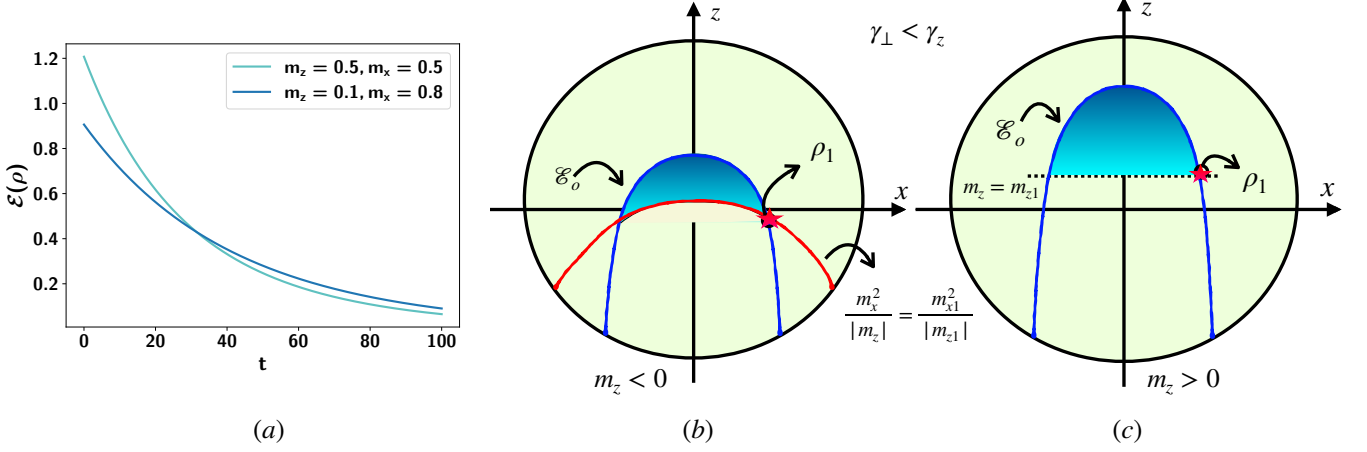


FIG. 10. EMC region for anisotropic Pauli channel in the xz -plane. (a) $\mathcal{E}(\rho)$ vs t for two mixed states with $\{m_x = 0.5, m_z = 0.5\}$ and $\{m_x = 0.1, m_z = 0.8\}$. (b) The region in the xz -plane that show EMC with the reference state ρ_1 , marked in star. Two region emerges depending upon the m_z of the state ρ_1 , specifically, (b) $m_z < 0$ and (c) $m_z > 0$. The system parameters are $\gamma_\perp = 0.01$ and $\gamma_z = 0.001$.

In this case, the asymptotic decay of ergotropy is governed by the transverse magnetization m_x , and therefore by the coherence of the initial state. Using arguments analogous to those above, one finds that an ergotropic Mpemba crossing occurs whenever the initially higher-ergotropy state has smaller coherence, i.e.,

$$\mathcal{C}(\rho_1) < \mathcal{C}(\rho_2).$$

This completes the proof. \square

In Fig. 10(b) and (c), we depict the regions exhibiting ergotropic Mpemba crossings for a fixed reference state ρ_1 , considering initial states with $m_z < 0$ and $m_z > 0$ in the xz plane, respectively. For $m_z > 0$, we find that the line of constant magnetization $m_z = \text{const}$ forms the boundary of the EMC region, with the reference state ρ_1 located at the intersection of this line and an isoergotropic curve. Notably, the EMC region is significantly reduced for the anisotropic Pauli channel compared to the gADC case. In particular, unlike the gADC, no pair of pure states exhibits EMC under anisotropic Pauli noise. In contrast, when $m_z < 0$, the second term in Eq. (D2) becomes relevant, modifying both the shape and extent of the EMC region. In this regime, the boundary of the EMC region is jointly determined by the isoergotropic curve and the constraint $m_x^2/|m_z| = \text{const}$. These results clearly demonstrate the sensitivity of EMC to the initial-state parameters in the presence of anisotropic Pauli noise.

Coherent and incoherent ergotropy in anisotropic Pauli channel. Beyond the gADC, a similar qualitative behavior is observed for the anisotropic Pauli channel which can also be observed from Eq. (D1). In this case as well, a behavioral exchange between the coherent and incoherent contributions to ergotropy occurs for pairs of states that exhibit EMC. Unlike the gADC, however, the coherent ergotropy does not display

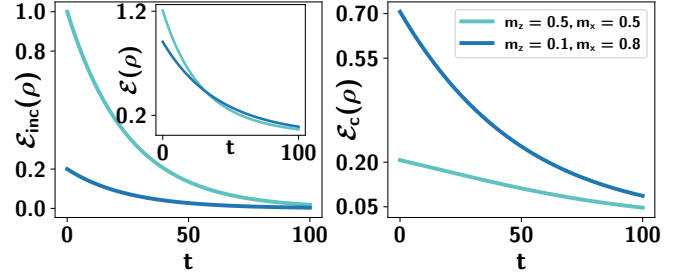


FIG. 11. Incoherent and coherent ergotropies against time for anisotropic Pauli channel. (a) Incoherent ergotropy and (b) coherent ergotropy is plotted against t . Unlike the gADC case, for anisotropic Pauli channel, coherent ergotropy decreases sharply. An exchange of behavior for the two different states is observed in coherent ergotropy which delays the saturation to the steady value of total ergotropy. Other parameters of the systems are $h_z = 1$, $\gamma_\perp = 0.01$ and $\gamma_z = 0.001$.

nonanalytic behavior in time, instead, it decreases sharply. Meanwhile, the coherent part of the ergotropy relaxes more slowly, while the incoherent part relaxes faster. The combined effect of these contrasting relaxation behaviors gives rise to ergotropic Mpemba crossings, as illustrated in Fig. 11(a) and (b).

Appendix E: Non-Markovian evolution of a qubit battery and the ergotropy

In this section, we provide the details of the non-Markovian evolution of a single qubit where the entire system and environment are evolved by the interaction Hamiltonian, given in Eq. 24. Now, we take an ansatz, given in Eq. (25) and put it in

the Schrodinger equation which is given as

$$i\dot{\nu}(t) = \sum_k \eta_k(t) g_k e^{i(2h_z - \omega_k)t}$$

$$i\dot{\eta}_k(t) = \nu(t) g_k^* e^{-i(2h_z - \omega_k)t}, \quad (\text{E1})$$

where we have taken $\hbar = 1$. Now, the solution of the above coupled equation can be obtained easily which is given as

$$\dot{\nu}(t) = -i \sum_k \eta_k(t) g_k e^{i(2h_z - \omega_k)t}$$

$$= - \sum_k g_k g_k^* \int_0^t \nu(t') e^{-i(2h_z - \omega_k)t'} dt' \cdot e^{i(2h_z - \omega_k)t}$$

$$= - \sum_k |g_k|^2 \int_0^t \nu(t') e^{i(2h_z - \omega_k)(t-t')} dt'$$

$$= - \int_0^t K(t-t') \nu(t') dt', \quad (\text{E2})$$

where in the second line we have used the fact that $\eta_k(t) = -i g_k^* \int_0^t \nu(t') e^{-i(2h_z - \omega_k)t'} dt'$. Now, performing a Laplace transformation in both side of the above equation, we obtain

$$s\tilde{\nu}(s) - \nu(0) = -\tilde{K}(s)\tilde{\nu}(s)$$

$$\Rightarrow \tilde{\nu}(s)[s + \tilde{K}(s)] = \nu(0)$$

$$\tilde{\nu}(s) = \frac{\nu(0)}{s + \tilde{K}(s)}$$

$$= \frac{\alpha}{s + \tilde{K}(s)}. \quad (\text{E3})$$

Now in order to obtain $\nu(t)$, we again perform inverse Laplace transform, which is given as

$$|\nu(t)| = e^{-\frac{\lambda t}{2}} \left| \alpha \left(\cosh \left(\frac{\zeta t}{2} \right) + \frac{\lambda - i\Delta}{\zeta} \sinh \left(\frac{\zeta t}{2} \right) \right) \right|, \quad (\text{E4})$$

where $\zeta^2 = (\lambda - i\Delta)^2 - 2\gamma\lambda$. Now tracing out the environment, the evolved state of the system is given in Eq. 26 and the eigenvalues of the evolved state is given as

$$\frac{1}{2} \left(1 - \sqrt{1 - 4|\alpha\nu|^2 + 4|\alpha\nu|^4 + 4|\beta|^2|\alpha\nu|^2} \right)$$

$$\frac{1}{2} \left(1 + \sqrt{1 - 4|\alpha\nu|^2 + 4|\alpha\nu|^4 + 4|\beta|^2|\alpha\nu|^2} \right). \quad (\text{E5})$$

Now using the eigenvalues of the evolved state, we can easily find out the ergotropy of the state which is given as

$$\mathcal{E}(t) = h_z (-1 + 2|\alpha\nu|^2)$$

$$+ h_z \sqrt{1 - 4|\alpha\nu|^2 4|\alpha\nu|^4 + 4|\beta|^2|\alpha\nu|^2}. \quad (\text{E6})$$

Now as described in Sec. V, we can easily generalize this formulation to a mixed initial state, where an arbitrary single qubit mixed state is given as

$\rho_0 = \frac{1}{2} (I + \vec{m} \cdot \vec{\sigma}) = \lambda_+ |\psi_+\rangle \langle \psi_+| + \lambda_- |\psi_-\rangle \langle \psi_-|$, with $\lambda_{\pm} = \frac{1}{2} (1 \pm |\vec{m}|)$, and $|\psi_+\rangle = \cos(\frac{\theta}{2}) |0\rangle + e^{i\phi} \sin(\frac{\theta}{2}) |1\rangle$, and $|\psi_-\rangle = \sin(\frac{\theta}{2}) |0\rangle - e^{i\phi} \cos(\frac{\theta}{2}) |1\rangle$. Using the linearity of unitary and partial trace operation, we can add up the solutions for $|\psi_+\rangle$ and $|\psi_-\rangle$ and the evolved state is given as

$$\rho(t) = \lambda_+ \rho_+(t) + \lambda_- \rho_-(t),$$

where $\rho_+(0) = |\psi_+\rangle \langle \psi_+|$ and $\rho_-(0) = |\psi_-\rangle \langle \psi_-|$ and the total evolved state is given as

$$\rho(t) = \begin{pmatrix} (\lambda_+|\alpha_+|^2 + \lambda_-|\alpha_-|^2)|\nu|^2 & (\lambda_+\alpha_+\beta_+ + \lambda_-\alpha_-\beta_-)\nu \\ (\lambda_+\alpha_+^*\beta_+^* + \lambda_-\alpha_-^*\beta_-^*)\nu^* & 1 - (\lambda_+|\alpha_+|^2 + \lambda_-|\alpha_-|^2)|\nu|^2 \end{pmatrix}. \quad (\text{E7})$$

The eigenvalues of the evolved state are

$$\lambda_1 = \frac{1}{2} \left(1 - \sqrt{(2(\lambda_+|\alpha_+|^2 + \lambda_-|\alpha_-|^2)|\nu|^2 - 1)^2 + 4|(\lambda_+\alpha_+\beta_+ + \lambda_-\alpha_-\beta_-)\nu|^2} \right),$$

$$\lambda_2 = \frac{1}{2} \left(1 + \sqrt{(2(\lambda_+|\alpha_+|^2 + \lambda_-|\alpha_-|^2)|\nu|^2 - 1)^2 + 4|(\lambda_+\alpha_+\beta_+ + \lambda_-\alpha_-\beta_-)\nu|^2} \right).$$

using the eigenvalues of the state, one can easily calculate the ergotropy of the evolved state which is given as

$$\mathcal{E} = h_z (2(\lambda_+|\alpha_+|^2 + \lambda_-|\alpha_-|^2)|\nu|^2 - 1) + h_z \sqrt{(2(\lambda_+|\alpha_+|^2 + \lambda_-|\alpha_-|^2)|\nu|^2 - 1)^2 + 4|(\lambda_+\alpha_+\beta_+ + \lambda_-\alpha_-\beta_-)\nu|^2}. \quad (\text{E8})$$

and the ergotropy in terms of magnetization of the state is given as

$$\mathcal{E} = h_z (|\nu|^2 (1 + |\vec{m}| \cos \theta) - 1) + h_z \sqrt{(|\nu|^2 (1 + |\vec{m}| \cos \theta) - 1)^2 + |\vec{m}|^2 \sin^2 \theta |\nu|^2}. \quad (\text{E9})$$

1. Proofs for Lemma 3 and 4

In this subsection, we prove the lemma 3 for non-Markovian ergotropic Mpemba effect which is given as **Lemma 3.** *For two isoergotropic states, the ergotropy of the state with a larger magnetization along the z direction decays faster than that of the state with smaller m_z for non-Markovian evolution.*

Proof. In this proof, we again use the phase covariance of the channel and consider the ergotropy in the xz -plane. The ergotropy, in the xz -plane is given as

$$\mathcal{E}(t, m_x, m_z) = \frac{(|\nu|^2(1 + m_z) - 1)}{+\sqrt{(|\nu|^2(1 + m_z) - 1)^2 + m_x^2|\nu|^2}}. \quad (\text{E10})$$

Now using Eq. (9), one can write that $m_x^2 = \mathcal{E}_0^2 - 2\mathcal{E}_0 m_z$, where \mathcal{E}_0 is the constant ergotropic surface. After substituting this into Eq. (E10), we now prove that for a particular time t , the ergotropy decays monotonically with the increase of m_z on the isoergotropic surface. To do so, we compute the first order derivative of the ergotropy which is given as

$$\frac{\partial \mathcal{E}(t, m_z)}{\partial m_z} = |\nu|^2 \left(1 + \frac{A}{B} \right), \quad (\text{E11})$$

where $A \equiv |\nu|^2(1 + m_z) - 1 - \mathcal{E}_0$ and $B \equiv \sqrt{(|\nu|^2(1 + m_z) - 1)^2 + (\mathcal{E}_0^2 - 2\mathcal{E}_0 m_z)|\nu|^2}$. It is easy to find out that $|\nu|^2(1 + m_z) - 1 - \mathcal{E}_0 = |\nu|^2 - 1 + |\nu|^2 m_z - \mathcal{E}_0 < 0$, hence, $A < 0$ where $|\nu|^2 < 1$. Now $A^2 - B^2 = (\mathcal{E}_0^2 + 2\mathcal{E}_0)(1 -$

$|\nu|^2) > 0$. So it is also clear that $|\frac{A}{B}| > 1$. Hence, one can write

$$\frac{\partial \mathcal{E}(t, m_z)}{\partial m_z} < 0,$$

which proves that $\mathcal{E}(t, m_z)$ monotonicity decreases with increment of m_z on the isoergotropic surface. \square

Lemma 4. *For two non-isoergotropic states with identical m_x , the ergotropy of the state with a larger m_z decays more slowly than that of the state with a smaller m_z .*

Proof. In order to prove the above statement, we fix the value of $m_x = M_x$ and computing the derivative with respect to m_z , we obtain

$$\begin{aligned} \frac{\partial \mathcal{E}(t, m_z)}{\partial m_z} &= |\nu|^2 \left(1 + \frac{|\nu|^2(1 + m_z) - 1}{\sqrt{(|\nu|^2(1 + m_z) - 1)^2 + M_x^2|\nu|^2}} \right) \\ &\equiv |\nu|^2 \left(1 + \frac{C}{D} \right). \end{aligned} \quad (\text{E12})$$

Now, it is easy to show that $|\frac{C}{D}| < 1$ which indicates the following relation,

$$\frac{\partial \mathcal{E}}{\partial m_z} > 0.$$

This proves the lemma. \square

[1] E. B. Mpemba and D. G. Osborne, Cool?, *Physics Education* **4**, 172 (1969).

[2] Z. Lu and O. Raz, Nonequilibrium thermodynamics of the markovian mpemba effect and its inverse, *Proceedings of the National Academy of Sciences* **114**, 5083–5088 (2017).

[3] S. Liu, H.-K. Zhang, S. Yin, and S.-X. Zhang, Symmetry restoration and quantum mpemba effect in symmetric random circuits, *Phys. Rev. Lett.* **133**, 140405 (2024).

[4] X. Turkeshi, P. Calabrese, and A. De Luca, Quantum mpemba effect in random circuits, *Phys. Rev. Lett.* **135**, 040403 (2025).

[5] F. Ares, S. Murciano, and P. Calabrese, Entanglement asymmetry as a probe of symmetry breaking, *Nature Communications* **14**, 10.1038/s41467-023-37747-8 (2023).

[6] S. Yamashika, F. Ares, and P. Calabrese, Entanglement asymmetry and quantum mpemba effect in two-dimensional free-fermion systems, *Phys. Rev. B* **110**, 085126 (2024).

[7] S. Murciano, F. Ares, I. Klich, and P. Calabrese, Entanglement asymmetry and quantum mpemba effect in the xy spin chain, *Journal of Statistical Mechanics: Theory and Experiment* **2024**, 013103 (2024).

[8] F. Ares, P. Calabrese, and S. Murciano, The quantum mpemba effects, *Nature Reviews Physics* **7**, 451–460 (2025).

[9] F. Carollo, A. Lasanta, and I. Lesanovsky, Exponentially accelerated approach to stationarity in markovian open quantum systems through the mpemba effect, *Phys. Rev. Lett.* **127**, 060401 (2021).

[10] A. K. Chatterjee, S. Takada, and H. Hayakawa, Multiple quantum mpemba effect: Exceptional points and oscillations, *Phys. Rev. A* **110**, 022213 (2024).

[11] M. Moroder, O. Culhane, K. Zawadzki, and J. Goold, Thermodynamics of the quantum mpemba effect, *Phys. Rev. Lett.* **133**, 140404 (2024).

[12] A. Nava and R. Egger, Mpemba effects in open nonequilibrium quantum systems, *Phys. Rev. Lett.* **133**, 136302 (2024).

[13] A. K. Chatterjee, S. Takada, and H. Hayakawa, Multiple quantum mpemba effect: Exceptional points and oscillations, *Phys. Rev. A* **110**, 022213 (2024).

[14] D. Qian, H. Wang, and J. Wang, Intrinsic quantum mpemba effect in markovian systems and quantum circuits, *Phys. Rev. B* **111**, L220304 (2025).

[15] E. L. Caldas and D. P. Pires, Exponentially accelerated relaxation and quantum mpemba effect in open quantum systems (2025), arXiv:2512.07561 [quant-ph].

[16] R. F. Saliba and R. C. Drumond, Unraveling the quantum mpemba effect on markovian open quantum systems (2025), arXiv:2512.13509 [quant-ph].

[17] I. Ulčakar, R. Sharipov, G. Lagnese, and Z. Lenarčič, Conserved quantities enable the quantum mpemba effect in weakly open systems (2025), arXiv:2511.16739 [quant-ph].

[18] D. J. Strachan, A. Purkayastha, and S. R. Clark, Non-markovian

quantum mpemba effect, *Phys. Rev. Lett.* **134**, 220403 (2025).

[19] S. Longhi, Quantum mpemba effect from initial system-reservoir entanglement, *APL Quantum* **2**, 10.1063/5.0266143 (2025).

[20] S. Kochsiek, F. Carollo, and I. Lesanovsky, Accelerating the approach of dissipative quantum spin systems towards stationarity through global spin rotations, *Phys. Rev. A* **106**, 012207 (2022).

[21] J. W. Dong, H. F. Mu, M. Qin, and H. T. Cui, Quantum mpemba effect of localization in the dissipative mosaic model, *Phys. Rev. A* **111**, 022215 (2025).

[22] Z. Wei, M. Xu, X.-P. Jiang, H. Hu, and L. Pan, Quantum mpemba effect in dissipative spin chains at criticality (2025), arXiv:2508.18906 [quant-ph].

[23] A. Das, P. Chaki, P. Ghosh, and U. Sen, Role reversal in quantum mpemba effect (2025), arXiv:2512.24839 [quant-ph].

[24] A. K. Chatterjee, S. Takada, and H. Hayakawa, Quantum mpemba effect in a quantum dot with reservoirs, *Phys. Rev. Lett.* **131**, 080402 (2023).

[25] X. Wang and J. Wang, Mpemba effects in nonequilibrium open quantum systems, *Phys. Rev. Res.* **6**, 033330 (2024).

[26] A. Nava and R. Egger, Mpemba effects in open nonequilibrium quantum systems, *Phys. Rev. Lett.* **133**, 136302 (2024).

[27] S. Longhi, Bosonic mpemba effect with non-classical states of light, *APL Quantum* **1**, 10.1063/5.0234457 (2024).

[28] S. Longhi, Mpemba effect and super-accelerated thermalization in the damped quantum harmonic oscillator, *Quantum* **9**, 1677 (2025).

[29] D. J. Strachan, A. Purkayastha, and S. R. Clark, Non-markovian quantum mpemba effect, *Phys. Rev. Lett.* **134**, 220403 (2025).

[30] Y. Li, W. Li, and X. Li, Ergotropic mpemba effect in non-markovian quantum systems, *Phys. Rev. A* **112**, 032209 (2025).

[31] Z.-Z. Zhang, H.-G. Luo, and W. Wu, Quantum mpemba effect induced by non-markovian exceptional point (2026), arXiv:2511.13173 [quant-ph].

[32] R. Bao, Initial-state typicality in quantum relaxation, *Phys. Rev. Lett.* , (2026).

[33] X. Li, Y. Li, and Y. Yan, Canonical quantum mpemba effect in a dissipative qubit (2025), arXiv:2511.16996 [quant-ph].

[34] P. Bagui, A. Chatterjee, and B. K. Agarwalla, Detection of mpemba effect through good observables in open quantum systems (2025), arXiv:2512.02709 [cond-mat.stat-mech].

[35] P. Solanki, I. Lesanovsky, and G. Perfetto, Universal relaxation speedup in open quantum systems through transient conditional and unconditional resetting (2025), arXiv:2512.10005 [cond-mat.stat-mech].

[36] T. Lejeune, M. Papić, J. Goold, F. C. Binder, F. Damanet, and M. Moroder, Accelerating qubit reset through the mpemba effect (2026), arXiv:2602.03765 [quant-ph].

[37] L. K. Joshi, J. Franke, A. Rath, F. Ares, S. Murciano, F. Kranz, R. Blatt, P. Zoller, B. Vermersch, P. Calabrese, C. F. Roos, and M. K. Joshi, Observing the quantum mpemba effect in quantum simulations, *Phys. Rev. Lett.* **133**, 010402 (2024).

[38] A. Chatterjee, S. Khan, S. Jain, and T. S. Mahesh, Direct experimental observation of quantum mpemba effect without bath engineering (2025), arXiv:2509.13451 [quant-ph].

[39] B. P. Schnepper, J. L. D. de Oliveira, C. H. S. Vieira, K. Zawadzki, and R. M. Serra, Experimental observation and application of the genuine quantum mpemba effect (2025), arXiv:2511.14552 [quant-ph].

[40] R. Alicki and M. Fannes, Entanglement boost for extractable work from ensembles of quantum batteries, *Phys. Rev. E* **87**, 042123 (2013).

[41] F. C. Binder, S. Vinjanampathy, K. Modi, and J. Goold, Quantacell: powerful charging of quantum batteries, *New Journal of Physics* **17**, 075015 (2015).

[42] F. Campaioli, F. A. Pollock, F. C. Binder, L. Céleri, J. Goold, S. Vinjanampathy, and K. Modi, Enhancing the charging power of quantum batteries, *Phys. Rev. Lett.* **118**, 150601 (2017).

[43] D. Ferraro, M. Campisi, G. M. Andolina, V. Pellegrini, and M. Polini, High-power collective charging of a solid-state quantum battery, *Phys. Rev. Lett.* **120**, 117702 (2018).

[44] G. M. Andolina, M. Keck, A. Mari, M. Campisi, V. Giovannetti, and M. Polini, Extractable work, the role of correlations, and asymptotic freedom in quantum batteries, *Phys. Rev. Lett.* **122**, 047702 (2019).

[45] G. Francica, F. C. Binder, G. Guarneri, M. T. Mitchison, J. Goold, and F. Plastina, Quantum coherence and ergotropy, *Phys. Rev. Lett.* **125**, 180603 (2020).

[46] H.-L. Shi, S. Ding, Q.-K. Wan, X.-H. Wang, and W.-L. Yang, Entanglement, coherence, and extractable work in quantum batteries, *Phys. Rev. Lett.* **129**, 130602 (2022).

[47] S. Julià-Farré, T. Salamon, A. Riera, M. N. Bera, and M. Lewenstein, Bounds on the capacity and power of quantum batteries, *Phys. Rev. Res.* **2**, 023113 (2020).

[48] X. Yang, Y.-H. Yang, M. Alimuddin, R. Salvia, S.-M. Fei, L.-M. Zhao, S. Nimmrichter, and M.-X. Luo, Battery capacity of energy-storing quantum systems, *Phys. Rev. Lett.* **131**, 030402 (2023).

[49] B. Mohan and A. K. Pati, Reverse quantum speed limit: How slowly a quantum battery can discharge, *Phys. Rev. A* **104**, 042209 (2021).

[50] B. Mohan and A. K. Pati, Quantum speed limits for observables, *Physical Review A* **106**, 10.1103/physreva.106.042436 (2022).

[51] D. Shrimali, B. Panda, and A. K. Pati, Stronger speed limit for observables: Tighter bound for the capacity of entanglement, the modular hamiltonian, and the charging of a quantum battery, *Phys. Rev. A* **110**, 022425 (2024).

[52] S. Ghosh, T. Chanda, S. Mal, and A. Sen(De), Fast charging of a quantum battery assisted by noise, *Phys. Rev. A* **104**, 032207 (2021).

[53] S. Zakavati, F. T. Tabesh, and S. Salimi, Bounds on charging power of open quantum batteries, *Phys. Rev. E* **104**, 054117 (2021).

[54] M. B. Arjmandi, H. Mohammadi, and A. C. Santos, Enhancing self-discharging process with disordered quantum batteries, *Phys. Rev. E* **105**, 054115 (2022).

[55] K. Sen and U. Sen, Noisy quantum batteries (2023), arXiv:2302.07166 [quant-ph].

[56] S.-Q. Liu, L. Wang, H. Fan, F.-L. Wu, and S.-Y. Liu, Better performance of quantum batteries in different environments compared to closed batteries, *Phys. Rev. A* **109**, 042411 (2024).

[57] S. Ahuja, T. K. Konar, and A. S. De, Enhancing work-extraction in quantum batteries via correlated reservoirs (2025), arXiv:2509.25109 [quant-ph].

[58] S. Tirone, R. Salvia, S. Chessa, and V. Giovannetti, Work extraction processes from noisy quantum batteries: The role of nonlocal resources, *Phys. Rev. Lett.* **131**, 060402 (2023).

[59] S. Tirone, R. Salvia, S. Chessa, and V. Giovannetti, Quantum work capacitances: Ultimate limits for energy extraction on noisy quantum batteries, *SciPost Phys.* **17**, 041 (2024).

[60] S. Tirone, R. Salvia, S. Chessa, and V. Giovannetti, Quantum work extraction efficiency for noisy quantum batteries: The role of coherence, *Phys. Rev. A* **111**, 012204 (2025).

[61] A. Sarkar, P. Chaki, P. Ghosh, and U. Sen, Fluctuation in energy extraction from quantum batteries: How open should the system be to control it? (2025), arXiv:2505.16851 [quant-ph].

[62] F. H. Kamin, F. T. Tabesh, S. Salimi, F. Kheirandish, and A. C. Santos, Non-markovian effects on charging and self-

discharging process of quantum batteries, *New Journal of Physics* **22**, 083007 (2020).

[63] A. C. Santos, Quantum advantage of two-level batteries in the self-discharging process, *Phys. Rev. E* **103**, 042118 (2021).

[64] K. Xu, H.-G. Li, H.-J. Zhu, and W.-M. Liu, Inhibiting the self-discharging process of quantum batteries in non-markovian noises, *Phys. Rev. E* **109**, 054132 (2024).

[65] D. Morrone, M. A. Rossi, and M. G. Genoni, Daemonic ergotropy in continuously monitored open quantum batteries, *Phys. Rev. Appl.* **20**, 044073 (2023).

[66] M. Hadipour and S. Haseli, *Nonequilibrium quantum batteries: Amplified work extraction through thermal bath modulation* (2025), arXiv:2502.05508 [quant-ph].

[67] I. Medina, O. Culhane, F. C. Binder, G. T. Landi, and J. Goold, Anomalous discharging of quantum batteries: The ergotropic mpemba effect, *Phys. Rev. Lett.* **134**, 220402 (2025).

[68] S. Mondal and U. Sen, Mpemba effect in self-contained quantum refrigerators: accelerated cooling (2025), arXiv:2507.15811 [quant-ph].

[69] P. Chattopadhyay, J. F. G. Santos, and A. Misra, *Anomaly to resource: The mpemba effect in quantum thermometry* (2026), arXiv:2601.05046 [quant-ph].

[70] T. Van Vu and H. Hayakawa, Thermomajorization mpemba effect, *Phys. Rev. Lett.* **134**, 107101 (2025).

[71] A. Summer, M. Moroder, L. P. Bettmann, X. Turkeshi, I. Marvian, and J. Goold, A resource-theoretical unification of mpemba effects: classical and quantum, *Phys. Rev. X*, (2026).

[72] F. Carollo, A. Lasanta, and I. Lesanovsky, Exponentially accelerated approach to stationarity in markovian open quantum systems through the mpemba effect, *Phys. Rev. Lett.* **127**, 060401 (2021).

[73] A. E. Allahverdyan, R. Balian, and T. M. Nieuwenhuizen, Maximal work extraction from finite quantum systems, *Europhysics Letters (EPL)* **67**, 565–571 (2004).

[74] A. H. A. Malavazi, B. Ahmadi, P. Horodecki, and P. R. Dieguez, *Charge-preserving operations in quantum batteries* (2025), arXiv:2510.25549 [quant-ph].

[75] M. A. Nielsen and I. L. Chuang, *Quantum computation and quantum information* (Cambridge university press, 2010).

[76] H. P. Breuer and F. Petruccione, *The Theory of Open Quantum Systems* (Oxford University Press, Oxford, 2002).

[77] A. Rivas and S. F. Huelga, *Open Quantum Systems: An Introduction* (SpringerBriefs in Physics, Springer, Spain, 2012).

[78] A. H. Malavazi, R. Sagar, B. Ahmadi, and P. R. Dieguez, Two-time weak-measurement protocol for ergotropy protection in open quantum batteries, *PRX Energy* **4**, 023011 (2025).

[79] J. Furtado and A. C. Santos, Enhanced quantum mpemba effect with squeezed thermal reservoirs, *Annals of Physics* **480**, 170135 (2025).

[80] S. Lorenzo, F. Plastina, and M. Paternostro, Geometrical characterization of non-markovianity, *Phys. Rev. A* **88**, 020102 (2013).

[81] J. A. Gyamfi, Fundamentals of quantum mechanics in liouville space, *European Journal of Physics* **41**, 063002 (2020).